1997

Development of Radiation Shielding Materials for Space Applications

Stephen C. Ko
College of William & Mary - Arts & Sciences

Development of Radiation Shielding Materials for Space Applications

---

A Thesis

Presented to

The Faculty of the Department of Chemistry

The College of William and Mary

In Partial Fulfillment

of the Requirements for the Degree of

Master of Arts

---

by

Stephen C. Ko

1997

APPROVAL SHEET

This thesis is submitted in partial fulfillment of

the requirements for the degree of

Master of Arts

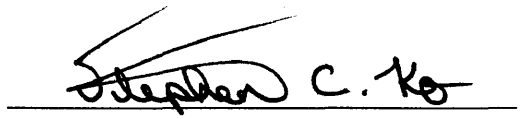

Stephen C. Ko

Approved, August 1997

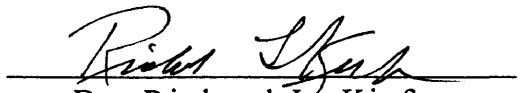

Dr. Richard L. Kiefer
Committee Chairman/Thesis Advisor

Dr. Robert A. Orwoll

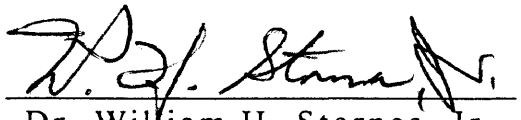

Dr. William H. Starnes, Jr.

Table of Contents

ACKNOWLEDGMENTS

This work was supported by the NASA Space Exploration Initiative, NASA grant NCC-1-239, and the Department of Chemistry of the College of William and Mary.

I would like to express my heartfelt appreciation to Dr. Kiefer for his guidance, patience, and trust throughout this research. I thank Dr. Orwoll and Dr. Starnes for their criticism of the thesis. I am very grateful to Dr. Thibeault and Glenn King for their help at the Langley Research Facility.

I would also like to thank several individuals whose help will not soon be forgotten: Dr. McDaniel, Janice, Jim, Craig, Theresa, Hoi, Pert, Peggy, Shirley, and all others who made thoughtful contributions. My sincerest thanks to all my friends: John, Brandon, David, Jenny, Judy, Joann, Angela, Melysa, Rachel, Olivia, Denisse, Jung-En, Christina, Nancy, and many others. Special thanks to Jamie whose love and support during the summer made it one of the most unforgettable of my life.

I would like to thank my mother, father, and sister for their support, love, and trust throughout all my endeavors. I could not ask for a better family. Finally, I would like to thank the Lord for all the blessings that I have in my life.

List of Tables

List of Figures

ABSTRACT

This work involved the development of radiation shielding materials for space applications. Specifically, amorphous boron powder and boron carbide whiskers were incorporated into the polymer matrixes of two polyimides. These two polyimides were NASA LaRC PETI-5 and Dupont K3B. The resulting samples were characterized physically, thermally, and mechanically. PETI-5 was successfully fabricated with both amorphous boron powder and boron carbide whiskers. Addition of amorphous boron powder and boron carbide whiskers did not affect the thermal performance of the polymers. The addition of boron carbide whiskers enhanced the compressive properties of the PETI-5. PETI-5 with the addition of boron carbide whiskers showed great promise as a candidate for radiation shielding space applications.

Chapter I.

Introduction

I.I. Background

As we approach the twenty-first century, worldwide interest in space exploration is at a peak. With increased cooperation between nations in their pursuit to broaden the global horizon, space travel and space exploration is extending beyond the moon. Joint projects, such as the Mir space station, now allow humans to stay in space for extended periods of time.

As such, radiation-shielding materials are significant for future space endeavors. These radiation-shielding materials will protect humans and electronic equipment from highly penetrating radiation during space travel. Cosmic radiation can have adverse effects on both humans and electronics. Figure 1.1 shows the effects of highly penetrating galactic cosmic rays on the space helmets worn by Apollo 12 astronauts.[1]

Although radiation shielding materials are of primary

importance to space exploration, they are also vital in several other areas such as nuclear energy related applications and high altitude, high speed aircraft. They could be utilized in nuclear energy plants in containing radiation from nuclear disasters such as Chernobyl. They could also be used in high-speed commercial planes. Since these aircraft fly at altitudes notably higher than those of normal aircraft, they experience enhanced cosmic radiation. In short, wherever harmful radiation exists, there will be a need for radiation shielding materials.

I.II. Cosmic Radiation

The two major sources of highly damaging and penetrating space radiation are solar particle events and galactic cosmic rays.[2] Solar particle events (solar flares) consist primarily of protons with energies less than 1 GeV. The total radiation flux from solar events is dependent on solar activity cycles. These cycles influence the levels of sunspot activity and magnitude of solar flare energies.[3]

Galactic cosmic rays are the source of the more deleterious space radiation. They consist of nuclei with

energies as high as 10^{10} GeV.[4] Galactic cosmic radiation comes from two primary sources, extragalactic space radiation and intragalactic space radiation. They are composed of highly damaging charged particles, with the more intense of the two being intragalactic radiation.

Galactic cosmic radiation (GCR) consists primarily of protons, electrons, positrons, and alpha particles. Protons make up 70% of GCR while alpha particles make up 20%. However, 0.6% of GCR constitutes heavier particles which can inflict the most damage to living systems as well as electronics on board spacecraft.[5] These heavier particles can interact with the atomic nuclei of the spacecraft and transfer energy by Coulombic processes. The energy transferred by such Coulombic processes increases as the square of the atomic number of the charged particle. This is why these heavier charged particles can transfer enormous amounts of energy to polymeric materials that comprise spacecraft. Since these high energy, high charge particles have a preference for lighter nuclei, hydrogen-containing polymers such as polyethylene are very effective as shielding materials.

Galactic cosmic radiation particles reacting with spacecraft nuclei also cause cascade reactions. These cascade

reactions give rise to several secondary particles, such as protons and neutrons. These particles can then react with the spacecraft materials.[6] Figure 1.2 illustrates the cascade reactions caused by protons and alpha particles. Positively charged secondary protons are stopped effectively by Coulombic interactions with matter. However, uncharged secondary neutrons only lose energy by inelastic collision or by reacting with an atomic nucleus. Atomic nuclei can then further reduce the energy of these neutrons by elastic collision. Atomic nuclei absorb these slow or thermal neutrons, with a probability called the cross section.[7] Lighter nuclei absorb a larger percentage of the kinetic energy from neutrons during elastic collisions. This is why hydrogen containing polymers are very effective materials in reducing the energy of neutrons in addition to interacting with high energy, high charge nuclei. Once highly energetic neutrons are slowed to thermal energies, there is a high probability of neutron capture reactions with target nuclei. This is significant since the products of such reactions are often radioactive.[8]

Secondary particles can cause significant damage to spacecraft materials and humans. With the advent of the Mir space station, extended exposure to galactic cosmic radiation

and secondary particles from cascade reactions could increase the likelihood of cancer risk in human bodies. Calculations show that a deep space journey to Mars would destroy 0.1% of the cerebral cortex.[9] The thermal and mechanical properties of polymers which comprise spacecraft hulls could also be compromised. In addition, sensitive electronic devices in spacecraft could undergo single event upsets.[10]

Since the effects of galactic cosmic radiation cannot be experimentally determined without extended missions to the outer reaches of space, scientists at the Langley Research Center of NASA and cooperating universities developed computer models and transport codes to estimate the flux of space radiation and its impact on materials. Employing a heavy ion/nucleon transport code for space radiation (HZETRN), Kim calculated the effects of heavy ions on a variety of shielding materials. In her dissertation, Kim concluded that shielding materials should provide adequate shielding from galactic cosmic rays. In addition, she determined that boron-containing polymers showed promise in their ability to absorb secondary neutrons from cascade reactions of incident galactic radiation.[11]

I.III. Neutron Interaction Theory

Nuclear reactions occur when an incoming particle interacts with a target nucleus. The resulting reaction could give rise to elastic or inelastic scattering of the particle, transformation of the target nucleus to another nuclide involving gain or loss of subatomic particles, and a variety of other possibilities. The probability that such a reaction will occur is related to the concept of reaction cross section signified by the Greek letter sigma, σ. In order for nuclear reactions to occur, the incoming particle must come within close proximity to the target nucleus. In some cases the centers of the projectile and nucleus must come within a distance R_{target} from each other for a reaction to occur. In this case, the geometrical cross section of the target nucleus can be calculated with the simple equation shown below.

$$\sigma_{geometric} = \pi (R_{target})^2$$

In this way the cross section of the target nucleus is related to

the size of the target nucleus (R_{target}). This simplified equation provides a good estimate of cross section, although more accurate cross sections take into account other factors such as target nucleus stability, projectile size, projectile energy, and projectile identity. The geometric cross section units are reported in barns, which are equivalent to $1x10^{-24}cm^2$. Cross sections may represent the overall probability of reaction of the target nucleus or they may represent specific reaction channels.[12]

Data for target nucleus cross sections are usually reported for thermal neutron capture cross sections. This is the capture of thermal (slow) neutrons by target nuclei. Since they are slow moving, thermal neutrons have the highest cross sections of all neutron species. For neutron interactions, neutron capture cross sections become lower with increasing neutron energy. This is illustrated in Figure 1.3.[13].

In Figure 1.3, resonance spikes can also be seen. These resonance spikes correspond to specific energy levels. Fortuitously, ^{10}boron has a resonance for thermal neutrons, since it is at exactly one of the resonance levels. Therefore, it has an unusually high neutron capture cross section.

In this work, neutrons act as incoming projectiles while

boron is the target nucleus. This is fortuitous since the data for target nuclei cross sections are usually reported for thermal neutron capture cross sections. This means differing target nuclei are bombarded with a flux of thermal neutrons.

Since thermal neutrons have high cross sections, there is a high probability that they will interact with matter onboard spacecraft and subsequently cause damage. Direct interactions of thermal neutrons and target species often result in the emission of a γ ray. In this type of radiative capture, the thermal neutron is captured by a nucleus resulting in an excited state that de-excites by emission of the γ ray. This work concentrates on the use of ^{10}B, which is an isotope with 19.8% natural abundance. In particular, it has a high thermal neutron capture cross section, listed as 3838 barns.[14] In this neutron interaction, ^{10}B reacts with a neutron to form ^{11}B. ^{11}Boron then spontaneously breaks apart to form an excited state of ^{7}Li and ^{4}He. A gamma ray is also released as lithium de-excites from its excited state. This is shown in Figure 1.4.

I.IV. Boron Carbide Whiskers

In this work, there were two materials used for the inclusion of boron into the polymer matrix. Both materials were purchased from Johnson Matthey. The first material was amorphous boron powder. It was a 325 mesh material with 99.99% purity. The second material was boron carbide whiskers. These whiskers were 300 microns in length and 5-8 microns in diameter.

The boron carbide whiskers were of particular interest since they are the ultimate in short fiber reinforcements. The technology of whiskers and short fibers is one that could possibly afford advantages in retaining or even improving the mechanical properties of polymeric materials while enhancing their radiation shielding capabilities. The following is an overview of whisker technology.

Whiskers are the premium in short fibers since they are single crystal fibers with a high degree of crystalline perfection. Compared to polycrystalline fibers and polycrystalline rods, they have fewer surface and internal

imperfections and lower void content. For a comparison, see Figure 1.5.[15] As such, they offer higher mechanical properties and a high degree of nonfriability and toughness. This toughness is needed for processing purposes.

When fibers are chopped, milled, blended, or mixed they are usually severely weakened. This reduces their aspect ratio, or length to diameter ratio. Aspect ratios in the range of 30 to 50 are preferred.[16] Generally, the smaller the whisker the stronger it is. However, if the whisker is too small, there will be a significant increase in surface area. Therefore, it may be difficult to wet and evenly distribute the fibers. Ideally, small whiskers, 4 to 6 microns in diameter are best.

I.V. Polyimides

Polyimides are a group of condensation polymers exhibiting excellent thermal and mechanical properties along with oxidative stability. They are formed from the reaction of bifunctional carboxylic acid anhydrides with primary diamines. The imide group can be either heterocyclic or linear along the polymer's backbone.

Polyimides are found in a wide variety of applications. These include the electrical, automotive, and aerospace industries. They are considered specialty plastics due to their remarkable properties and stability.

Dupont was a major proponent during the invention and development of polyimides during the 1950's. One of their first successful polyimides was a film based on ODA (oxydianiline) and PMDA (pyromellitic dianhydride). By the mid 1960's Dupont had developed three major polyimide products, Kapton (a film), Pyre-ML (wire insulation), and Vespel (molding).

Currently, scientific and commercial interest in polyimides has stimulated creative research in the field. In addition to Dupont, such companies as Occidental, Mitsui-Toatsu, and government agencies such as NASA have made valuable contributions.

In this work, two different polyimides were used. The first was a phenylethynyl terminated polyimide from the NASA Langley Research Center (LaRC). It is designated LaRC PETI-5. In the past few years, researchers have studied ethynyl terminated oligomers and used their cured resins in a number of applications. NASA Langley scientists recently developed

phenylethynyl endcaps, which offer distinct advantages over the ethynyl endcaps. The phenylethynyl group is better able to endure harsh conditions during synthesis due to its thermal and chemical stability.[17] PETI-5 is based on BPDA (3,3',4,4'-biphenyltetracarboxylic dianhydride), an 85/15 ratio of ODA (3,4'-oxydianiline) to APB (1,3-bis(3-aminophenoxy)benzene), and PEPA (4-phenylethynylphthalic anhydride) as an endcapper.[18] Figure 1.6 illustrates the synthetic route follwed in making PETI-5.

The second material was a thermoplastic polyimide provided by Dupont. From a patent on the chemical formulation of the polymer, it was difficult to obtain information on the synthesis and structure of the polyimide. However, Dupont reported the glass transition temperature of the thermoplastic to be 459°F. In addition, the density of the material was reported to be 1.336 g/cm^3.

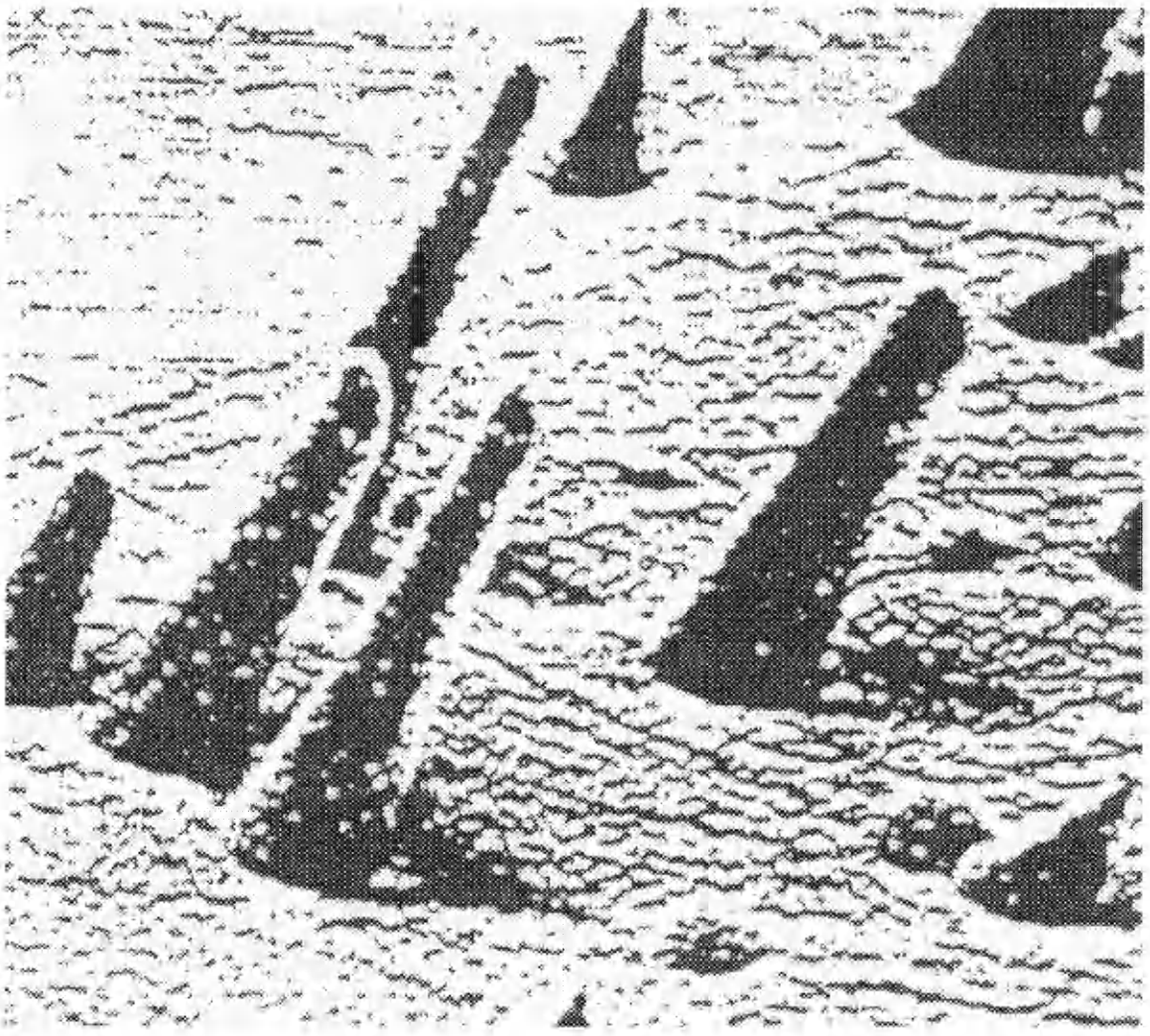

Figure 1.1
Radiation Effects on Helmets Worn
by Apollo 12 Astronauts

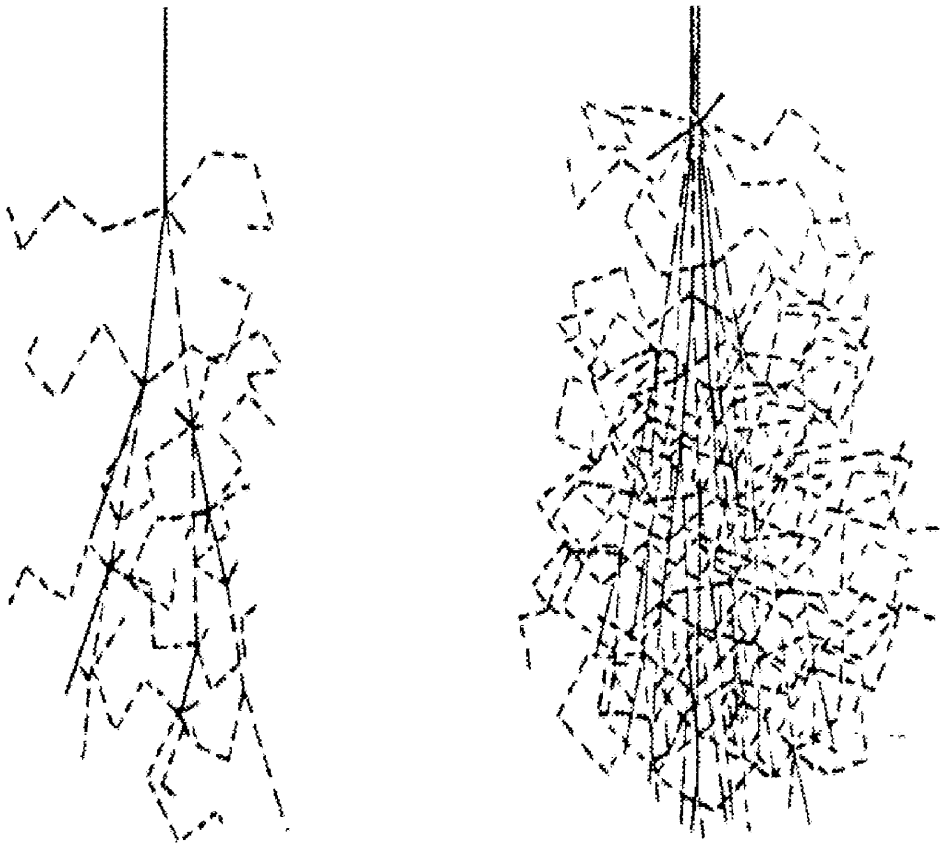

Figure 1.2
Cascade Reactions

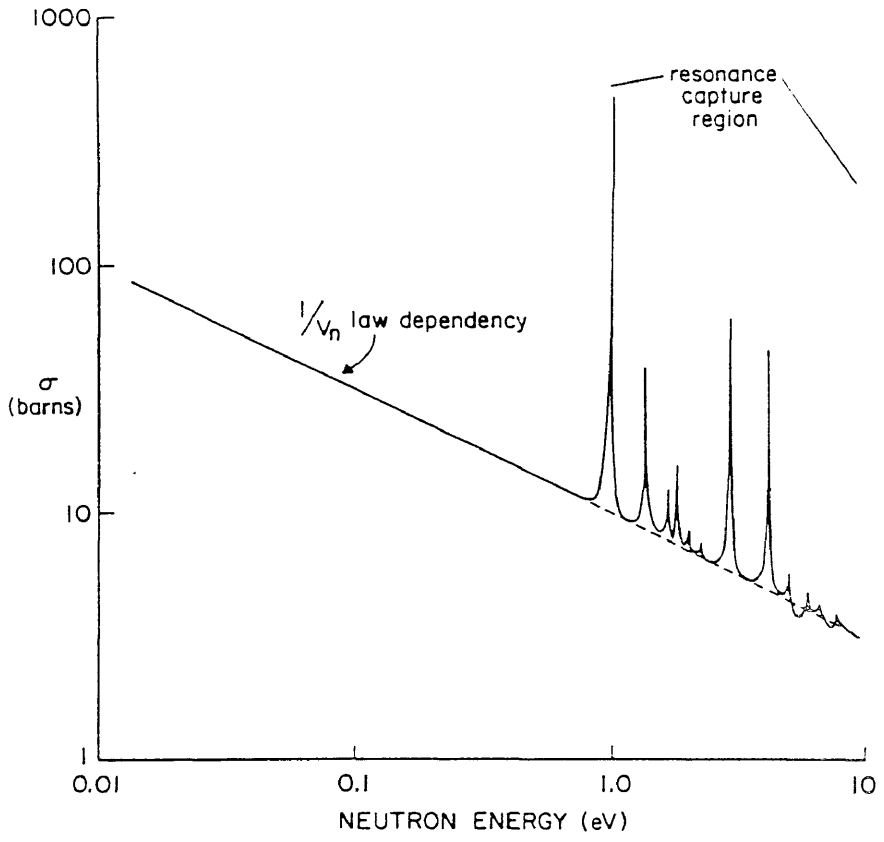

Figure 1.3
Neutron Capture Cross Section
vs. Neutron Energy

$$^{10}B + {}^{1}n \rightarrow {}^{11}B \rightarrow {}^{7}Li + {}^{4}He + 2.4MeV$$

Figure 1.4
Neutron Capture Theory

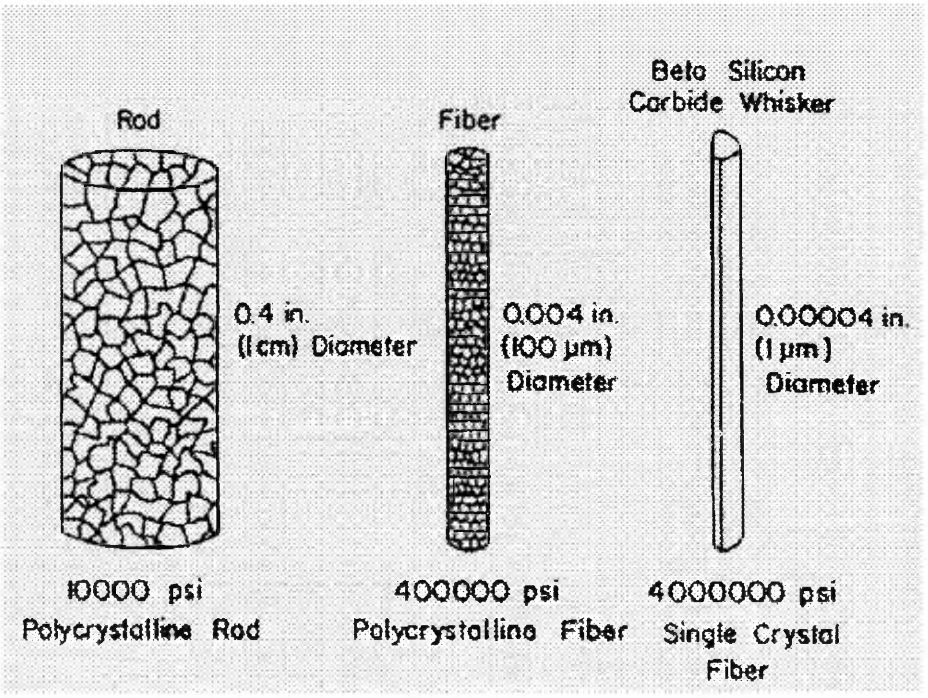

Figure 1.5
Whisker Perfection

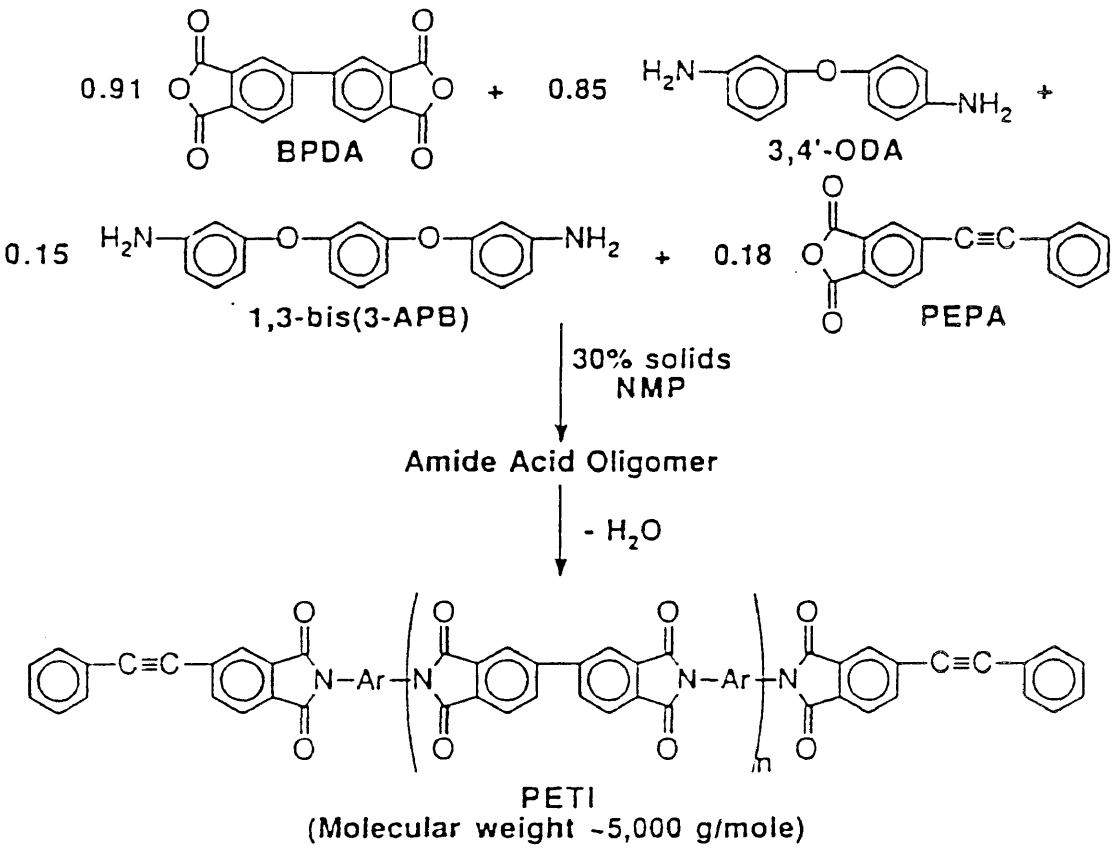

Figure 1.6
PETI-5 Synthesis

Literature Cited

[1] Ogura, B.L.: "Synthesis and Characterization of Poly(Carborane-Sulfone)," M.A. thesis, College of William and Mary, p. 3, 1996.

[2] Townsend, L.W.; Nealy, J.E. ; Wilson, J. W.; and Simonsen, L. C.: Estimates of Galactic Cosmic Ray Shielding Requirements During Solar Minimum. NASA TM-4167, p. 1, 1990.

[3] Glasgow, M.B.: "Synthesis and Characterization of Boron-Containing Polymeric Materials for Neutron Shielding Applications," doctoral thesis, College of William and Mary, p. 2, 1996.

[4] Kiefer, R.L.; Orwoll, R. A.: "The Development of Materials for Structures and Radiation Shielding in Space," grant proposal for NASA & William and Mary, p. 4, 1996.

[5] Choppin, G.R.; and Rydberg, J.: Nuclear Chemistry, p. 78, Pergamon Press, New York, 1990.

[6] Stephens, J.M.; Glasgow, M.B.; Kiefer, R.L.; Orwoll, R.A.; and Thibeault, S.A.: Polymer Preprints, vol. 33 (1) , p. 1152 (1992).

[7] Glasgow, p. 6.

[8] Kraus, W.B.; Glasgow, M.B.; Kim, M.Y.; Olmeijer, D.L.; Kiefer, R.L.; and Orwoll, R.A.: Polymer Preprints, vol. 34 (1), p. 592 (1993).

[9] Choppin, Chapter 5.

[10] Glasgow, p. 7.

[11] Kim, M.Y.: "Calculations of the Interactions of Energetic Ions with Materials for Protection of Computer Memory and Biological Systems," doctoral thesis, College of William and Mary, 1995.

[12] Ehmann, W.D.; and Vance, D.E.: Radiochemistry and Nuclear Methods of Analysis, pp. 90-92, Wiley and Sons, New York, 1991.

[13] Ibid, pp. 96-97.

[14] Friedlander, G.; Kennedy, J.W.; Macias, E.S.; and Miller, J.M.; Nuclear and Radiochemistry, 3rd ed., p. 610, John Wiley & Sons, New York, 1981.

[15] Milewski, John: Polymer Composites, vol. 13, no. 3, p. 224 (1992).

[16] Ibid, pp. 223-224

[17]Jensen, B.J.; Bryant, R.G.; Smith, J.G.; and Hergenrother, P.M.; Journal of Adhesion, vol.54, pp. 57-58 (1995).

[18] Ibid, pp. 58-59.

Chapter II.

Experimental Studies

II.I. Boron Inclusion

In theory there are at least two ways of adding boron to polymers. The first way involves the synthesis and addition of boron-containing groups into the polymer backbone. Both Glasgow and Ogura attempted this method. In his research, Glasgow synthesized m-carborane polyamides. Successful during the synthesis of the carborane polyamides, Glasgow encountered problems with low molecular weight yields upon characterization.[1] Ogura endeavored to synthesize carborane-based polysulfones. Unfortunately, her various attempts at condensation polymerization using 1,2-bis(hydroxymethyl)-O-carborane (BHMC) as a monomer and using disodium salts were unsuccessful. Some of her later attempts at synthesis using phase transfer catalysts showed promise near the end of her research.[2]

The second method of adding boron to polymers involves

the physical mixing of boron with polymers. This is done before crosslinking or molding of the polymer and involves the incorporation of boron into the polymer matrix. Glasgow successfully fabricated boron-containing epoxy materials in his research.[3] In this work, this latter method of physical mixing was the chosen method of boron inclusion.

In this work, amorphous boron powder and boron carbide whiskers were incorporated into polyimides. Both materials were purchased from Johnson Matthey Corporation. Elemental boron has a melting point of 2100°C and a boiling point of 2600°C. Its density is 2.34g/cm^3. Its crystal structure is hexagonal. The amorphous boron powder purchased from Johnson Matthey was reported to be of 99.99% purity.

The boron carbide whiskers had a boron content of 77-78%. They were typically 5-8 microns in diameter and 300 microns in length. The aspect ratio was 50, and the purity was reported as 99+%. The melting point of the whiskers was reported as 2350°C.

II.II. Processing and Fabrication

The polyimides PETI-5 and K3B were both purchased in powder form. PETI-5 was purchased from Imitec Corporation, and K3B was purchased from Dupont. Both powders were of a yellowish hue. Once received, the powders were vacuum dried for forty-eight hours at 100°C. The amorphous boron powder and the boron carbide whiskers were also vacuum dried for forty-eight hours at 100°C.

Amorphous boron powder was added to PETI-5 powder in weight percentages of ten and twenty percent. The powders were thoroughly mixed in a glass bottle to ensure uniform distribution. The resulting mixture turned gray due to the black hue of the amorphous boron powder. This mixture was then transferred to a 3.5 x 0.75 inch steel mold used to make samples for testing. The mold was coated with two layers of a hydrocarbon-based release agent, Freekote 44N, before the mixture of powders was added. The mold was rapidly heated in a press to 350°C, at which point 200 psi was applied. For this mold, roughly 524 pounds of pressure were needed. The temperature was raised to 371°C and held constant for 1 hour with the pressure applied while the thermoset crosslinked. The

temperature was lowered and the pressure was released after the temperature reached 155°C. For a heating profile of PETI-5 refer to Figure 2.1. Two samples of thickness 0.125 inch were made for each of the aforementioned concentrations of amorphous boron powder and for the pure powder. These samples were used for thermal tests. Two additional samples of each type with a thickness of 0.3 inch were made for mechanical tests. The same procedure was repeated using boron carbide whiskers instead of amorphous boron powder.

The amorphous boron powder and boron carbide whiskers were also added to Dupont K3B in weight percentages of ten and twenty percent. The K3B and boron powder (or boron carbide whiskers) were thoroughly mixed in a glass bottle to ensure uniform distribution. The same 3.5 x 0.75 inch steel mold was used to make samples for testing. Again, the mold was coated with Freekote 44N before the addition of the mixture. The heating profile of the K3B differed from that of the PETI-5. As a thermoplastic instead of a thermoset like PETI-5, a stop was needed to prevent the melted material from being forced out of the mold. After addition of the mixture, the mold was rapidly heated to 350°C. At this point, pressure was applied until the stops were reached. Then the mold was cooled

under pressure to room temperature. For a heating profile refer to Figure 2.2. The same four samples (per concentration of amorphous boron powder and boron carbide whiskers) were made using this procedure. In addition, samples of pure K3B were made.

II.III. Physical Characterization

Ultrasound

The samples were analyzed by ultrasound at NASA Langley. The ultrasonic data provided information on the structural integrity of the samples. The scans revealed the presence or absence of voids in the materials.

The ultrasound scans were made by using a Panametrics ultrasonic C-scan analyzer. The analyzer was coupled to Sonix software. The transducer frequency was set at 5 Mhz. The transducer had a focal length of 4 inches and a diameter of 0.5 inches. It was focused off the back surface of the specimen. The attenuation was set initially at 24dB. A Raster scan pattern was used. The scan length was 2 inches, and the scan

width was 1 inch. Data were obtained for every 0.01 inches along the scan length, and the transducer was indexed 0.01 inches between the scan lengths. Figure 2.3 illustrates the transducer set-up.

Photomicrographs

A light microscope was used to view the cut and uncut surfaces of the molded samples. The microscope was connected to a data acquisition system, and the images were saved. Polaroid 53 film was also used to develop photomicrographs. The photomicrographs provided a closer look at the surface of the samples.

II.IV. Thermal Characterization

A series of thermal tests was conducted on the samples to examine the thermal stability of the materials before and after addition of amorphous boron powder or boron carbide whiskers. As per ASTM E473 and ICTAC (International Confederation for Thermal Analysis and Calorimetry), thermal analysis refers to a

group of techniques in which the physical property of a material is measured as a function of time or temperature while the material is subjected to a controlled temperature program.[4]

Thermogravimetric Analysis

Thermogravimetric analysis (TGA) was performed on the samples to investigate stability of the materials under the duress of high temperatures. Samples were tested in air on a Shimadzu TGA-50 apparatus at the College of William and Mary.

In thermogravimetry, a change in sample weight is measured while the sample is heated or cooled at a constant rate. The mass of the sample is monitored by a thermobalance. For the Shimadzu TGA-50 instrument, the thermobalance was of the suspension type. The suspension mechanism was of low mass to ensure high sensitivity and resistance to vibration.

The samples, roughly 10 mg, were placed on platinum pans and subjected to a temperature program. The TGA curves were constructed from these heating profiles. The curves illustrated the resistance of the material to heat by tracking the

percent weight loss of the material versus temperature. Table 2.1 shows the heating program used for all samples.

Table 2.1
TGA heating profile for PETI-5 and K3B

Rate (C/min)	Hold Temperature (C)	Hold Time (min)
10.0	200.0	30.0
5.0	400.0	0.0
2.0	700.0	0.0
20.0	800.0	0.0

Differential Scanning Calorimetry

Differential scanning calorimetry (DSC) was used to determine the glass transition temperature of the samples. Samples were tested by using a Shimadzu DSC-50 instrument located at NASA Langley. The test methodology was in accordance with the procedure outlined in ASTM E1356.[5]

In this work, glass transition was defined as the change in

an amorphous material or in amorphous regions of partially crystalline materials to (or from) viscous or rubbery conditions to (or from) a brittle and relatively hard state. This definition was taken from ASTM E1142.[6]

For DSC, the glass transition temperature is derived from plots of heat capacity versus temperature. It is the temperature range at which there is a step in heat capacity. This "step" in heat capacity, with no heat accompanying it, is similar to a thermodynamic second order transition. However, since it depends on time it is not truly a thermodynamic transition.[7]

The DSC operated on a power compensated null balance principle. This principle involves the compensation of energy absorbed from a sample specimen by adding or subtracting an equivalent amount of energy from the sample holder. The constant adjustment of the heater power, which maintains the sample holder temperature equal to that of the reference pan, allows a fluctuation in electrical signal which is used to analyze the glass transition temperature. This electrical signal is proportional to the heat capacity of the specimen.[8]

Since the thermal history of the sample affects its DSC curve, each sample was run twice. Both runs were made at a rate of 20°C per minute to 400°C. The first heat provided a

representative curve of the sample's thermal history. After this first heat the sample was quenched, and a second heat was performed. This reheat provided repeatable baseline results which added reliability to the glass transition measurements. The actual glass transition temperatures were taken as the midpoint temperature instead of the extrapolated onset temperature. Per ASTM E1356, either the extrapolated onset temperature (T_f) or the midpoint temperature (T_m) could represent the temperature range over which the glass transition took place.[9] Representative graphs are in the Results and Discussion section.

Thermomechanical Analysis

Thermomechanical analysis (TMA) was conducted on the specimens to determine the softening point of the samples. Samples were tested on a Shimadzu TMA-50 apparatus located at the College of William and Mary. The test methodology was in accordance with ASTM E1545.[10]

For the TMA, a change in dimension of the sample is reported when the sample is subjected to a constant heating rate. This dimensional change is observed as the motion of the

sensing probe when it comes in direct contact with the sample. The detection probe, which is aligned with the differential transformer and force coil, ensures a high degree of accuracy in detecting dimensional changes. The softening point occurs at the intersection of slope of the probe displacement curve before and after the transition.[11]

TMA can be set up in a number of different modes. If a flat-tipped expansion probe is used while a negligible sample load is applied, the procedure is often referred to as linear thermodilatometry. When the set-up is this way, the temperature derived from this procedure is considered the glass transition temperature. The TMA can also be set up in penetration or compression mode. If the TMA is in penetration mode, the loss of rigidity of the material is considered the softening point.[12]

In this work, the TMA was set up in penetration mode. The softening temperature, T_s, was taken by constructing tangents to the slope of the penetration curve and marking the intersection of the tangents. The heating profile for the PETI-5 samples is shown in Table 2.2. The heating profile for the K3B samples is shown in Table 2.3. Representative graphs are in the Results and Discussion section.

ASTM E1545 states that the softening temperature is close to the glass transition temperature measured by expansion

Table 2.2
TMA heating profile for PETI-5 Samples

Rate (C/min)	Hold Temperature (C)	Hold Time (min)
5.0	180.0	30.0
2.0	300.0	0.0

Table 2.3
TMA heating profile for K3B Samples

Rate (C/min)	Hold Temperature (C)	Hold Time (min)
5.0	180.0	30.0
2.0	240.0	0.0

mode or by DSC. It is common practice for polymer laboratories to report the T_s as the T_g.[13]

II.V. Mechanical Characterization

Compression Tests

Compression tests were conducted on the specimens to determine mechanical properties of the samples under compression at uniform rates of load. The compression tests were conducted at NASA Langley. The test method was in accordance with the procedures of ASTM D695.[14]

From the two bars (per specimen) molded for mechanical testing, six samples were machined per specimen to dimensions of 1 inch x 0.5 inch x 0.3 inch. Each sample was fitted with four strain gages. Two strain gages were axial and two were transverse. In addition, an extensometer was attached to the sample. The samples were tested by using a Baldwin-Tate-Emery 120-kip (120,000 lb. full scale) universal test plant. This was coupled with a SATEC systems controller and an

Analogic ANDS 5400 data acquisition system to record the data from the extensometer and strain gages.

The procedure for the testing of the specimens follows. After measuring the width and thickness at several points along the sample, the minimum cross-sectional area was calculated. The length was also recorded. The samples were then loaded between the surfaces of the compression tool. Care was taken to ensure correct alignment of the sample. The crosshead of the compression tool was then adjusted until it contacted the specimen. No fixtures or grips were used. The strain gages and extensometer were then attached to the data acquisition system. Finally, the speed control was set at 0.05 inch per minute and the load was applied.

Real time stress vs. strain curves from the strain gages and extensometer were observed while the test was conducted. The data acquisition system recorded data from seven channels during each test. Channels 1 and 3 recorded data for axial strain, and channels 2 and 4 recorded data for transverse strain. Channel 5 recorded data for load. Channel 6 recorded data for crosshead. Channel 7 recorded data from the extensometer. The yield point for each specimen was noted from the real time stress-strain curves, and the test was stopped.

All data were copied and analyzed. Data reduction involved the use of Microsoft Excel. Stress vs. strain curves were created from the raw data for each of the six samples at differing concentrations of boron additives. From these curves, compressive yield strength was calculated. In addition, modulus of elasticity was calculated.

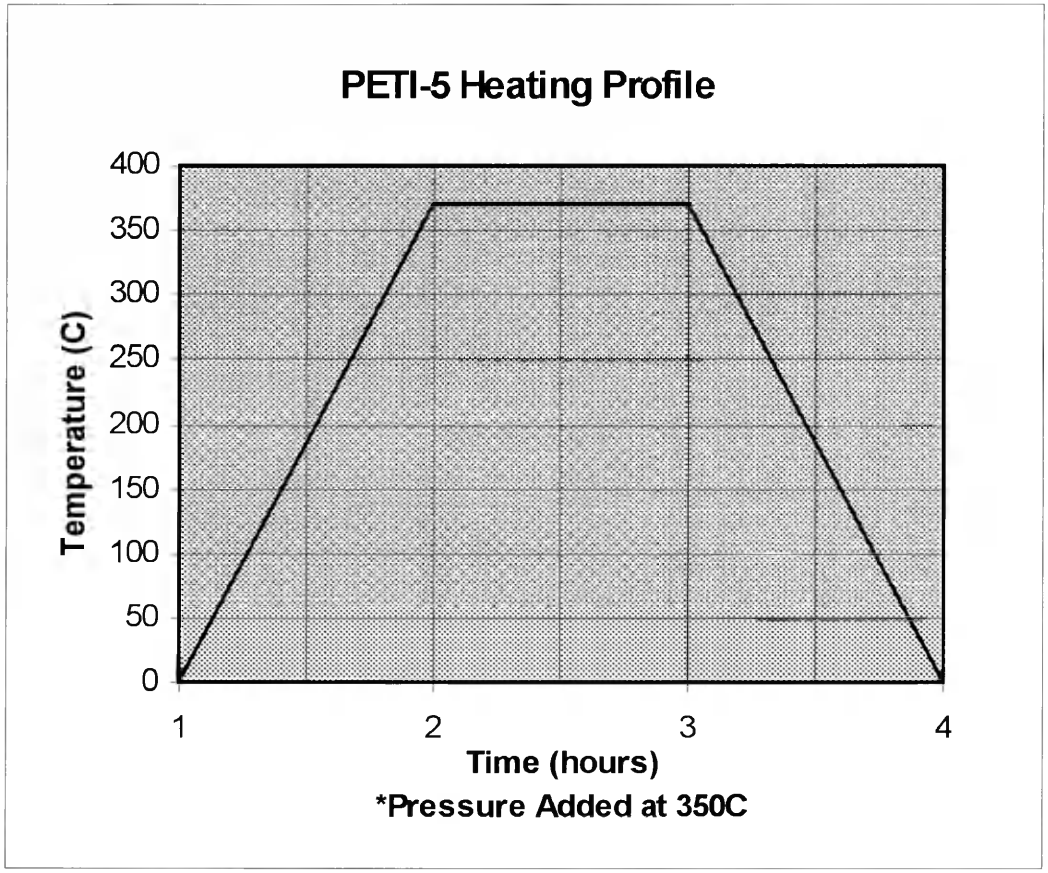

Figure 2.1
PETI-5 Temperature Profile
for Powder Processing

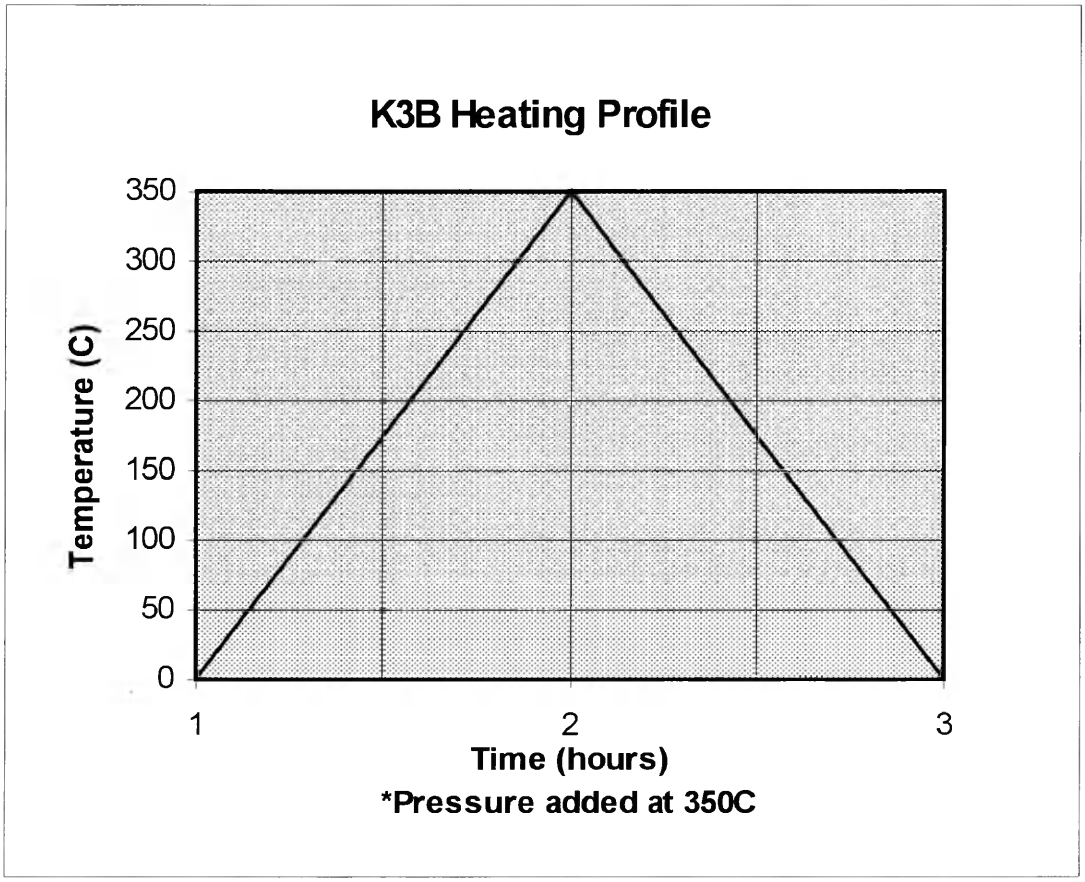

Figure 2.2
K3B Temperature Profile
for Powder Processing

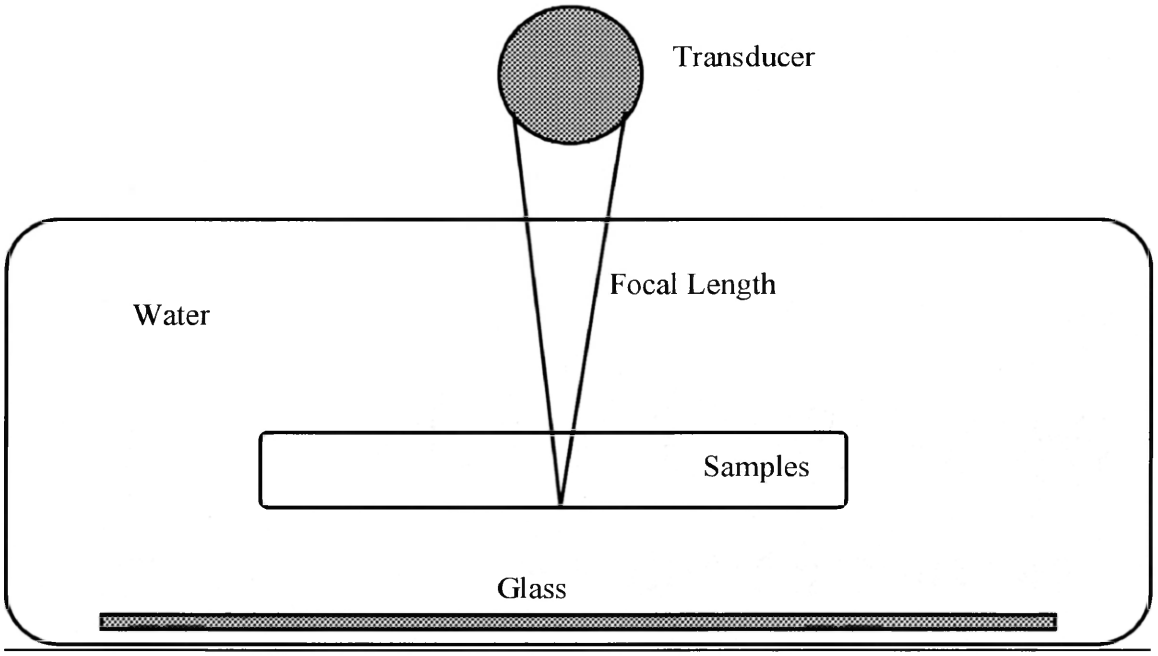

Figure 2.3
Simplistic Diagram of
Ultrasound Set-up

Literature Cited

[1] Glasgow, M.B.: "Synthesis and Characterization of Boron-Containing Polymeric Materials for Neutron Shielding Applications," doctoral thesis, College of William and Mary, p. 149, 1996.

[2] Ogura, B.L.: "Synthesis and Characterization of Poly(Carborane-Sulfone)," M.A., College of William and Mary, pp. 192-197.

[3] Glasgow, doctoral thesis.

[4] American Standard Test Method (ASTM E473).

[5] American Standard Test Method (ASTM E1356).

[6] American Standard Test Method (ASTM E1142).

[7] Bair, H.E.: "Glass Transition Measurements by DSC," Assignment of the Glass Transition, ASTM STP 1249, Philadelphia, 1994, pp. 50-74.

[8] Ibid, p. 51.

[9] American Standard Test Method (ASTM E1356).

[10] American Standard Test Method (ASTM E1545).

[11] Ibid, p. 990.

[12] Earnest, Charles: "Assignment of Glass Transition Temperatures Using Thermomechanical Analysis," Assignment of Glass Transition, ASTM STP1249, Philadelphia, 1994, pp. 75-87.

[13] ASTM E1545.

[14] American Standard Test Method (ASTM D695).

Chapter III.

Results and Discussion

III.I. Processing and Fabrication

Samples of PETI-5 and K3B were fabricated by the methods described in the experimental section. Table 3.1 shows the various concentrations of amorphous boron powder and boron carbide whiskers added to each sample. Two samples at each concentration were made for thermal testing and another two samples were fabricated for mechanical testing. All four

Table 3.1
Test Specimens

Material	Molded Samples	Weight Percent
PETI-5	Pure	NA
PETI-5	Amorphous Boron Powder	10%
PETI-5	Amorphous Boron Powder	20%
PETI-5	B_4C Whiskers	10%
PETI-5	B_4C Whiskers	20%
K3B	Pure	NA
K3B	Amorphous Boron Powder	10%
K3B	Amorphous Boron Powder	20%
K3B	B_4C Whiskers	10%
K3B	B_4C Whiskers	20%

samples were made by using the mold described in the experimental section.

The actual concentrations of boron in the samples were 7.9% amorphous boron for K3B and 7.8% amorphous boron for PETI-5 in the 10% category. For 20% the actual amorphous boron content was 14.8% for K3B and 16.2 % for PETI-5. This method of analysis was inductively coupled plasma measurements. The ICP method could not be used for the boron carbide whiskers, since they produced no residue after digestion.

The PETI-5 samples were fabricated with the temperature profile described in the experimental section. Most of the samples were made with relative ease. The pure PETI-5 samples turned dark brown after crosslinking. The material was solid and seemed to have no voids upon inspection.

The amorphous boron PETI-5 samples were difficult to release from the mold. Various methods were used to release the samples from the molds. These included the use of pressure, water, and additional coats of Freekote release agent. The most effective method was the addition of a layer of Kapton film between the sample and the mold plus coating with two layers of Freekote release agent. The molded samples containing amorphous boron seemed more brittle than the pure PETI-5

samples. The samples turned black after molding, and black powder particles came off on contact. Visual inspection showed that the samples had small pinhole voids on the surface. These voids were thought to result from the acrimonious attempts at releasing the samples from the mold.

The boron carbide PETI-5 samples were molded with the same technique used for the amorphous boron samples. With the addition of Kapton film around the samples and two layers of Freekote, the samples were easily removed from the molds. The finished samples looked dark brown upon visual inspection. Shiny points believed to be boron carbide whiskers could be seen on the surface. The samples were solid and contained no visible voids on the surface. They seemed to be more flexible than the pure PETI-5 samples and the brittle amorphous boron samples.

The Dupont K3B samples were molded with the technique described in the experimental section. There was great difficulty in obtaining samples without voids or imperfections. The pure K3B samples, although by no means perfect, seemed to yield the best results upon visual inspection. These samples were firm with only minor pinhole voids on the surface.

The amorphous boron K3B samples were the most difficult to fabricate. Upon addition of 10% amorphous boron, the

molded samples adhered tightly to the mold. This happened despite the use of a Kapton film and two layers of Freekote release agent. When the samples were finally freed from the mold, pieces fractured from the corners. The resulting sample was very friable. Numerous imperfections were apparent on the surface as were voids of various sizes.

Correspondence with the Dupont Corporation ensued after difficulty in processing the thermoplastic. Representatives at Dupont did not offer any helpful advice and were reluctant to divulge any information about the K3B material. They said that heating the thermoplastic under vacuum was not necessary. They also sent a copy of processing instructions. However, these processing instructions only described the exact way that the samples had been made.

Additional attempts were made at fabricating boron loaded samples without voids or imperfections. An effort was made to pack more powder into the mold. With some samples, so much material was added to the mold that upon reaching the softening point, more than half of the loaded material overflowed from the sides. Unfortunately, the finished samples still contained flaws. Other attempts were also fruitless in obtaining void-free, flawless samples.

When loading the K3B polymer with 20% of amorphous boron, the cured samples were even more difficult to remove from the molds. When the samples were finally pried from the mold, some of the samples cracked in half. The samples were extremely brittle and easily breakable. Boron powder rubbed off the samples upon physical contact. Most of the samples contained surface imperfections and voids.

Attempts were also made to incorporate boron carbide whiskers into the thermoplastic. The same difficulty in adhesion to the mold, although to a lesser extent, occurred with the boron carbide samples. The molded boron carbide samples were not as brittle as the amorphous boron samples. Instead of a black finish, the boron carbide loaded samples were dark brown. Like the PETI-5 samples, the K3B samples containing boron carbide whiskers seemed to be more pliable. Unfortunately, they did appear to have surface voids.

Since we were unable to fabricate samples without surface imperfections and voids, the best-looking samples identified with visual inspection were chosen for thermal and mechanical testing.

III.II. Physical Characterization

Photomicrographs

A light microscope with magnification up to 1500X was used to examine the cut and uncut surfaces of the molded samples. Attempts were made to find voids on the materials and to discriminate clumping of the amorphous boron or boron carbide whiskers in the samples.

The Dupont K3B samples were examined first to see how the surface imperfections and voids looked under a microscope. A magnification of 200X revealed voids evenly distributed over the surface of the cut and uncut samples. These voids, invisible to the naked eye, were clearly visible under a magnification of 200X. Under higher magnifications the microscope was able to focus in and out of the voids. Figure 3.1 illustrates the presence of porosity in the pure K3B samples.

Photomicrographs of K3B samples containing amorphous boron showed the same evidence of voids across the surface of

the material. Attempts were made to identify the presence of amorphous boron particles and to observe if clumping had occurred. Upon initial inspection of the samples, boron particles were not immediately identifiable. Colleagues at NASA Langley Research Center helped to identify small crystalline structures under the microscope. Some debate ensued as to whether the crystal structures were boron. The small crystal structures were not present in the pure K3B samples.

The added boron was described as amorphous by Johnson Matthey. Subsequently a call was made to Johnson Matthey to find out the meaning of this terminology. Johnson Matthey said that this meant that the boron powder, when subjected to an X-ray diffraction microscope, showed no signs of crystal formation. They also said that the -325 mesh descriptor meant that small boron particles could fit through a mesh if they were less than 44 microns in size.

In any case, if the small crystals were boron, they did not appear to be clumping. A few crystals were scattered in a random fashion across the surface of the samples. In Figure 3.2 there is a crystal particle in the lower left quadrant along with porosity.

Photomicrographs of Dupont K3B with boron carbide whiskers were also taken. Circular areas of porosity were apparent throughout the sample. Figure 3.3 gives an excellent view of these circular areas of porosity. In the background, boron carbide whiskers are also visible. However, a better look at the whiskers is available for the PETI-5 samples.

The PETI-5 samples were observed under the microscope at various magnifications. Photomicrographs of the pure PETI-5 samples indicated the absence of voids. Figure 3.4 is a photomicrograph of pure PETI-5. No voids or surface imperfections are visible.

The PETI-5 samples loaded with amorphous boron also yielded positive photomicrographs. Only a few tiny pinhole voids were visible across the surface. In looking at the samples, the same crystal structures present in the amorphous boron K3B samples were observed in the amorphous boron PETI-5 samples. These were randomly spread across the cut surface of the sample. Figure 3.5 is a photomicrograph focused on one of these crystal structures. A definite crystal lattice structure is visible with a magnification of 500X.

Finally, the PETI-5 samples loaded with boron carbide whiskers were examined under the microscope. There appeared to be no voids under magnifications up to 200X. Upon inspection at 200X, boron carbide whiskers were visible across the surface of the cut sample. These whiskers were randomly dispersed and did not exhibit any clumping. Figure 3.6 is an excellent illustration of the boron carbide whiskers found in the PETI-5 samples and also in the Dupont K3B samples.

Ultrasound

Ultrasonic C-scan analysis was performed on the samples to examine their structural integrity. The technique and apparatus were described in the experimental section.

The PETI-5 samples yielded ultrasonic scans which backed up the results found with the microscope. Strong signals resonated from the samples, indicating that the samples were solid throughout and contained no voids. Figure 3.7 is an ultrasound scan of pure PETI-5, while Figure 3.8 is an ultrasound scan of PETI-5 with 20% boron carbide whiskers.

Ultrasound analysis was also performed on the Dupont K3B samples. Unfortunately, the ultrasonic data backed up the

negative results from analysis by microscope. The worst samples either did not return noise to the transducer or returned noise at very faint signals. The sound was being lost within the sample. The samples were not solid throughout, and the noise was probably lost within voids in the material. Figures 3.9 and 3.10 show extreme examples of K3B samples with voids. Figure 3.9 is an ultrasound scan of pure K3B and Figure 3.10 is an ultrasound scan of K3B with 20% amorphous boron.

III.III. Thermal Characterization

Differential Scanning Calorimetry

DSC was performed on the samples in accordance with the procedures described in the experimental section. The glass transition temperatures were calculated by observing the midpoint temperatures (T_m) on the graphs. Two samples at each concentration in Table 3.1 were tested for their glass transition temperatures. The average of the results for the two samples was taken. Table 3.2 shows the results of the DSC tests. Figure

3.11 and Figure 3.12 are thermograms of pure PETI-5 and pure K3B respectively.

On a closer examination of Table 3.2, it was apparent that the addition of amorphous boron to the PETI-5 enhanced the glass transition temperature by a few degrees. The addition of boron carbide whiskers did not have a significant impact on the glass transition temperature. These trends are apparent in Figure 3.13.

Table 3.2
DSC Data

Compound	Tg	Avg. Tg
PETI-5 Pure	268.6	268.6
	268.6	
PETI-5 10% Amorphous Boron	274.4	271.8
	269.1	
PETI-5 20% Amorphous Boron	274.4	274.7
	275.0	
PETI-5 10% B4C Whiskers	270.1	269.6
	269.0	
PETI-5 20% B4C Whiskers	268.6	269.4
	270.1	
K3B Pure	234.3	235.0
	235.7	
K3B 10% Amorphous Boron	251.3	251.0
	250.6	
K3B 20% Amorphous Boron	243.8	243.9
	243.9	
K3B 10% Boron Carbide Whiskers	238.6	238.8
	238.9	
K3B 20% Boron Carbide Whiskers	239.1	239.8
	240.5	

The addition of amorphous boron to the K3B raised the glass transition temperature to a greater extent than seen for the PETI-5. Interestingly, the addition of 10% amorphous boron raised the glass transition temperature about 7 degrees more than the addition of 20% amorphous boron. An amount of boron loading somewhere between 10% and 20% is probably the limit of amorphous boron that can be added which does not have a detrimental effect on the polymer matrix of K3B. This is not true for boron carbide whiskers. Both levels of loading did not have a significant impact on the glass temperature of the K3B. These trends are illustrated in Figure 3.14.

Thermogravimetric Analysis

Thermogravimetric analysis was performed on the samples following the procedures indicated in the experimental section. Two samples at each concentration from Table 3.1 were tested. The temperature for five percent weight loss of all samples was reported. The averages of the data for the two samples at each concentration were then taken, and their standard deviation was calculated. Table 3.3 shows the results of the thermogravimetric analysis on all samples. Representative graphs of

thermogravimetric analysis for PETI-5 and K3B with 10% boron carbide whiskers are shown in Figures 3.15 and 3.16.

From the results of the thermogravimetric analysis, it is apparent that the addition of amorphous boron powder to the pure PETI-5 does not impede the thermal stability of PETI-5 according to thermogravimetric analysis. In fact, Figure 3.17

Table 3.3
TGA Data

Compound	5% Weight Loss	Average 5% Weight Loss
PETI-5 Pure	529.6	526.3
	523.0	
PETI-5 10% Amorphous Boron	550.8	551.6
	552.4	
PETI-5 20% Amorphous Boron	584.0	585.6
	587.2	
PETI-5 10% Boron Carbide Whiskers	520.6	523.3
	526.0	
PETI-5 20% Boron Carbide Whiskers	515.5	517.0
	518.5	
K3B Pure	507.6	508.4
	509.2	
K3B 10% Amorphous Boron	542.2	535.7
	529.2	
K3B 20% Amorphous Boron	553.4	552.6
	551.7	
K3B 10% Boron Carbide Whiskers	514.6	513.2
	511.7	
K3B 20% Boron Carbide Whiskers	514.7	516.9
	519.1	

shows that the addition of amorphous boron to PETI-5 increases the temperature for 5% weight loss of PETI-5.

With the addition of boron carbide whiskers to PETI-5, the temperature for 5% weight loss does not change significantly. Looking at Figure 3.17, one sees that the temperature for 5% weight loss of PETI-5 decreases by only a few degrees with the addition of 10% boron carbide whiskers. A possible reason for this slight decrease in weight loss is that the boron carbide whiskers oxidize between 500°C and 600°C. Since oxidation occurs at such high temperatures for the boron carbide whiskers, their addition does not really affect the thermal stability of the PETI-5. In fact, the boron carbide whiskers provide oxidation protection for polymers by oxidizing in carbon matrixes and forming glossy oxide protective layers.

The effects of addition of amorphous boron to pure K3B are shown in Figure 3.18. As with the PETI-5, the addition of the amorphous boron does not decrease the thermal stability of the K3B. It increases the temperature for 5% weight loss of the polymer.

The temperature for 5% weight loss of K3B does not change to a great extent with the addition of boron carbide

whiskers. Interestingly, the temperature for 5% weight loss increases by a few degrees instead of decreasing by a few degrees, as seen in the PETI-5. When comparing the thermal stability of pure K3B and PETI-5, it is apparent that the temperature for 5% weight loss of PETI-5 is about 20°C higher than that of K3B. Pure PETI-5 has a temperature for 5% weight loss of roughly 526°C, while for pure K3B this temperature is roughly 508°C. Therefore, the oxidation of the boron carbide whiskers probably occurs somewhere between the 508°C and 526°C.

Thermomechanical Analysis

Thermomechanical analysis was performed on all samples in accordance with the procedures described in the experimental section. Two samples from each concentration in Table 3.1 were tested. The softening point was taken for each sample, and the averages of the data for the two samples at each concentration were calculated. These are reported in Table 3.4. Representative TMA curves for PETI-5 and K3B with 20% amorphous boron are shown in Figures 3.19 and 3.20.

It is important to note that the softening points are significantly lower than the glass transition temperatures obtained with differential scanning calorimetry. It is true that glass transition temperatures can vary significantly when one is determining their values with different techniques. However, the TMA apparatus used in testing the samples had a problem with its temperature calibration. This problem caused results to be consistently 20°C lower than normal TMA values. This was

Table 3.4
TMA Data

Compound	Tg	Average Tg
PETI-5 Pure	232.6	232.5
	232.4	
PETI-5 10% Amorphous Boron	237.2	236.1
	234.9	
PETI-5 20% Amorphous Boron	236.1	238.2
	240.2	
PETI-5 10% Boron Carbide Whiskers	234.1	233.2
	232.3	
PETI-5 20% Boron Carbide Whiskers	232.8	232.3
	231.7	
K3B Pure	206.6	206.5
	206.4	
K3B 10% Amorphous Boron	215.9	217.0
	218.1	
K3B 20% Amorphous Boron	211.9	211.5
	211.0	
K3B 10% Boron Carbide Whiskers	208.6	207.7
	206.7	
K3B 20% Boron Carbide Whiskers	209.0	209.0
	208.9	

apparent in re-testing previously run TMA samples. This problem had not yet been corrected at the time of this publication. However, since the main purpose of the tests was to determine the qualitative effects of the addition of boron additives to polymers and not to determine the quantitative values for glass transition temperature, these data will still be reported. Instead, for quantitative data for glass transition temperatures, refer to the DSC data.

The softening points of the PETI-5 samples measured by TMA showed the same trends as the glass transition temperatures determined by DSC. For PETI-5 samples containing amorphous boron, the softening points increased a few degrees with the addition of amorphous boron. Boron carbide whiskers did not change the softening points of the PETI-5 samples. These trends are illustrated in Figure 3.21.

The softening points of the K3B samples also showed the same trends as the glass transition temperatures derived from the DSC data. The addition of 10% amorphous boron to K3B increased the softening point by a greater extent than the addition of 20% amorphous boron. This same phenomenon was seen with the DSC runs. The addition of boron carbide whiskers

did not affect the softening point of K3B to any great extent. These trends are displayed in Figure 3.22.

III.IV. Mechanical Characterization

Compression Tests

Compression tests were performed on all samples according to the procedures described in the experimental section. Two bars were molded for each of the concentrations in Table 3.1. From these two bars, six samples were machined to ASTM specifications. These samples were then fitted with strain gauges as described in the experimental section.

After machining the samples, it was apparent that the K3B samples contained significant amounts of porosity on the cut surfaces. This condition would probably affect the results of the compression tests. However, it was hoped that the results would still yield useful information. The PETI-5 samples did not have any voids.

After observing several compression runs, it was apparent that the strain gauges had gone beyond their limit of detection

(3% to 4%). Therefore, the compressive yield strength could not be evaluated with the raw data. It was then decided that an extensometer would be attached to the test specimens to record strain. For each test run, the strain gauges continued to record data to their limit of detection while the extensometer recorded data beyond this.

After acquisition of all data, stress vs. strain curves were formulated. A representative curve for pure PETI-5 is shown in Figure 3.23. The compressive yield strength was taken as the first point at which strain increased without a corresponding increase in stress. These values were calculated for five samples at each concentration of boron additive. The averages were then taken and the standard deviation calculated. Table 3.5 shows the results of these analyses for PETI-5 samples.

After examining the K3B data, it was determined that the data did not provide any useful information. Compressive yield strengths for the same sample concentrations differed by as much as 100%. This problem was due in part to the porosity of the material shown by the physical characterization.

The compressive chord modulus of elasticity was also calculated. This was taken as the slope of the initial linear portion of the stress vs. strain curve. The averages of data for

five samples were calculated and the standard deviation reported.

Table 3.5
Compression Yield Strength Data

Specimen	Min. Area (sq.in.)	Load at Yield Point (lbs)	Compressive Yield Strength (ksi)	Average Compressive Yield Strength (ksi)	Std. Dev.
1-1 (Pure)	0.1517	3601.2	23.74	23.20	1.18
1-2	0.1525	3676.2	21.11		
1-3	0.152	3473.0	22.85		
1-4	0.1522	3740.2	24.58		
1-5	0.1502	3564.4	23.73		
2-1 (10% A.B.)	0.1525	2692.5	17.66	18.24	2.26
2-2	0.1514	2365.6	15.63		
2-3	0.1519	3414.1	22.47		
2-4	0.1521	2696.3	17.73		
2-5	0.1519	2692.7	17.72		
3-1 (20% A.B.)	0.1527	2959.0	19.38	16.51	2.23
3-2	0.1523	2419.5	15.89		
3-3	0.1521	2413.9	15.87		
3-4	0.1526	1984.7	13.01		
3-5	0.1523	2806.2	18.42		
4-1 (10% Whis.)	0.1513	3726.7	24.63	24.61	0.12
4-2	0.1512	3693.3	24.43		
4-3	0.1518	3741.9	24.65		
4-4	0.1513	3749.4	24.78		
4-5	0.1519	3728.9	24.55		
5-1 (20% Whis.)	0.1522	3971.0	26.10	25.35	0.83
5-2	0.1522	3902.9	25.64		
5-3	0.152	3907.0	25.71		
5-4	0.1522	3894.0	25.58		
5-5	0.1515	3998.3	23.74		

The results of these analyses are in Table 3.6.

The ultimate compressive strength, calculated from the ultimate compressive load values, was not reported. It is believed that these values were close to the compressive yield strength. With the utilization of the extensometer, compressive loads were not extended beyond the limits of the yield point of the materials in fear of breaking the extensometer.

The analysis of the results showed that the addition of amorphous boron to the PETI-5 decreased the compressive yield strength of the polyimide. The yield strength decreased with increasing concentration of amorphous boron. This trend is illustrated in Figure 3.24. The compressive chord of elasticity decreased with the addition of 10% amorphous boron, but increased with the addition of 20% amorphous boron.

The addition of boron carbide whiskers improved the compressive properties of the PETI-5. The compressive yield strength increased with increasing concentration of boron carbide whiskers. The compressive chord of elasticity also increased with increasing concentration of boron carbide whiskers.

Table 3.6
Compressive Chord Modulus Data

Specimen	Compressive Chord Modulus of Elasticity (Msi)	Average Compressive Chord Modulus of Elasticity (Msi)	Std. Dev.
1-1 (Pure)	1.6530	1.6950	0.1222
1-2	1.5850		
1-3	1.7650		
1-4	1.8980		
1-5	1.5740		
2-1 (10% A.B.)	1.0230	1.5666	0.4066
2-3	1.3510		
2-4	2.0450		
2-5	1.3780		
2-6	2.0360		
3-1 (20% A.B.)	1.8270	1.8396	0.2846
3-3	1.4260		
3-4	1.9990		
3-5	1.6790		
3-6	2.2670		
4-1 (10% Whis.)	2.5800	2.4128	0.1024
4-2	2.4430		
4-3	2.3080		
4-4	2.4310		
4-5	2.3020		
5-1 (20% Whis.)	3.2750	2.9780	0.2596
5-2	2.5090		
5-3	3.0030		
5-4	3.1450		
5-5	2.9580		

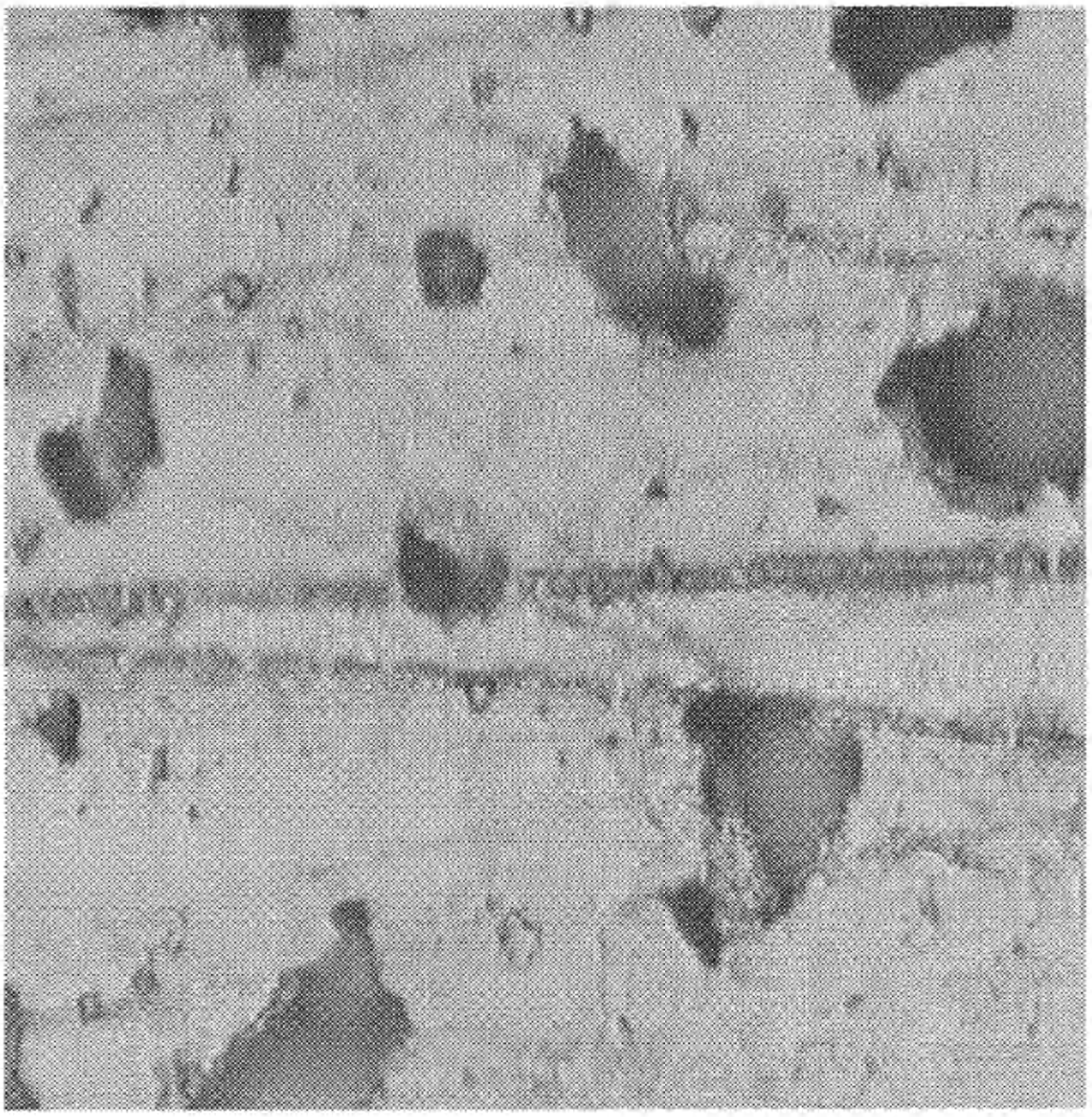

Figure 3.1 Photomicrograph of Dupont K3B (Pure)
Porosity is seen in this photomicrograph of Dupont K3B. (200X)

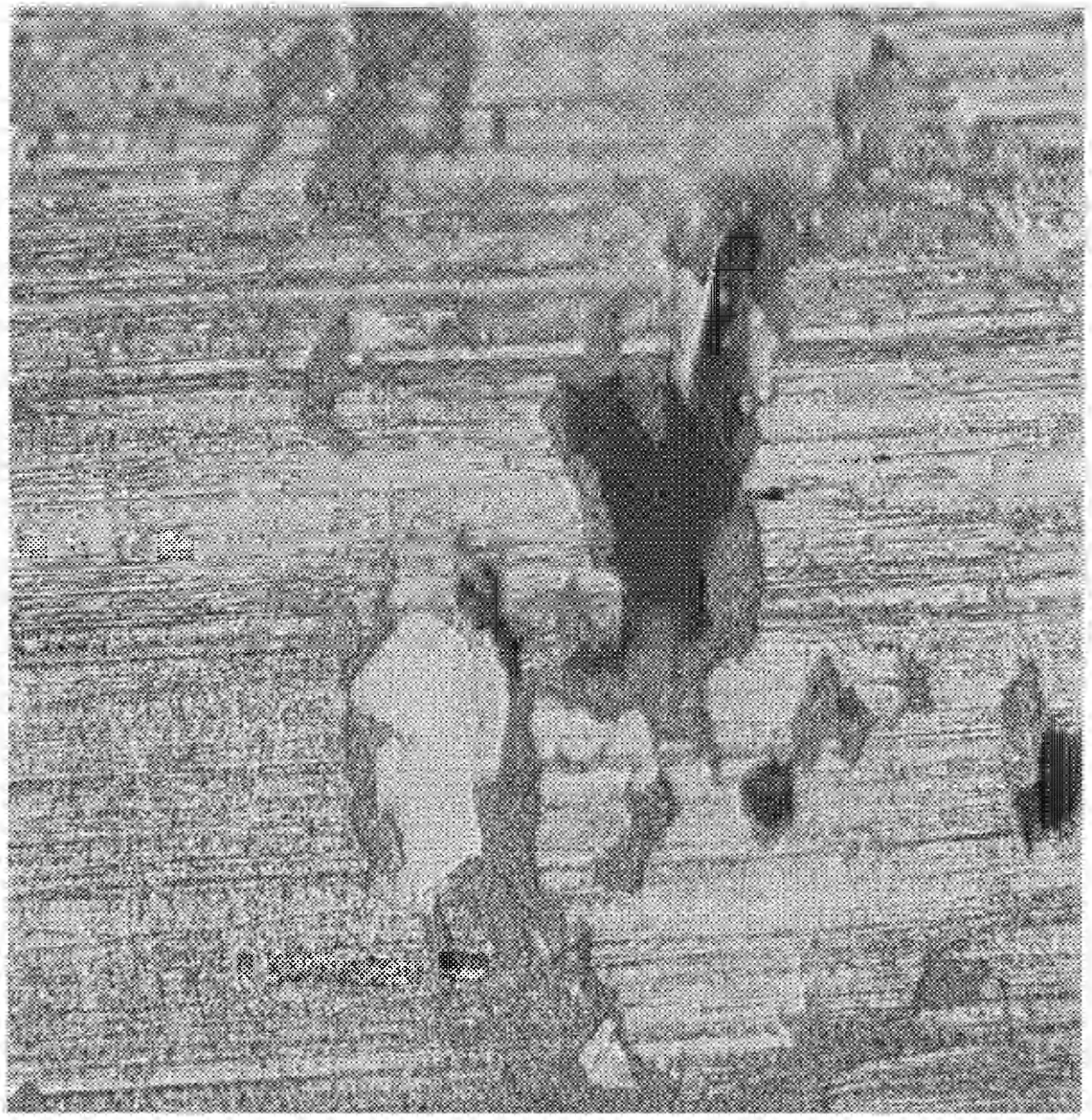

Figure 3.2 Photomicrograph of Dupont K3B with 20% Amorphous Boron
Porosity is seen in this photomicrograph of Dupont K3B. Also, a crystalline type structure, believed to be boron, is apparent. (200X)

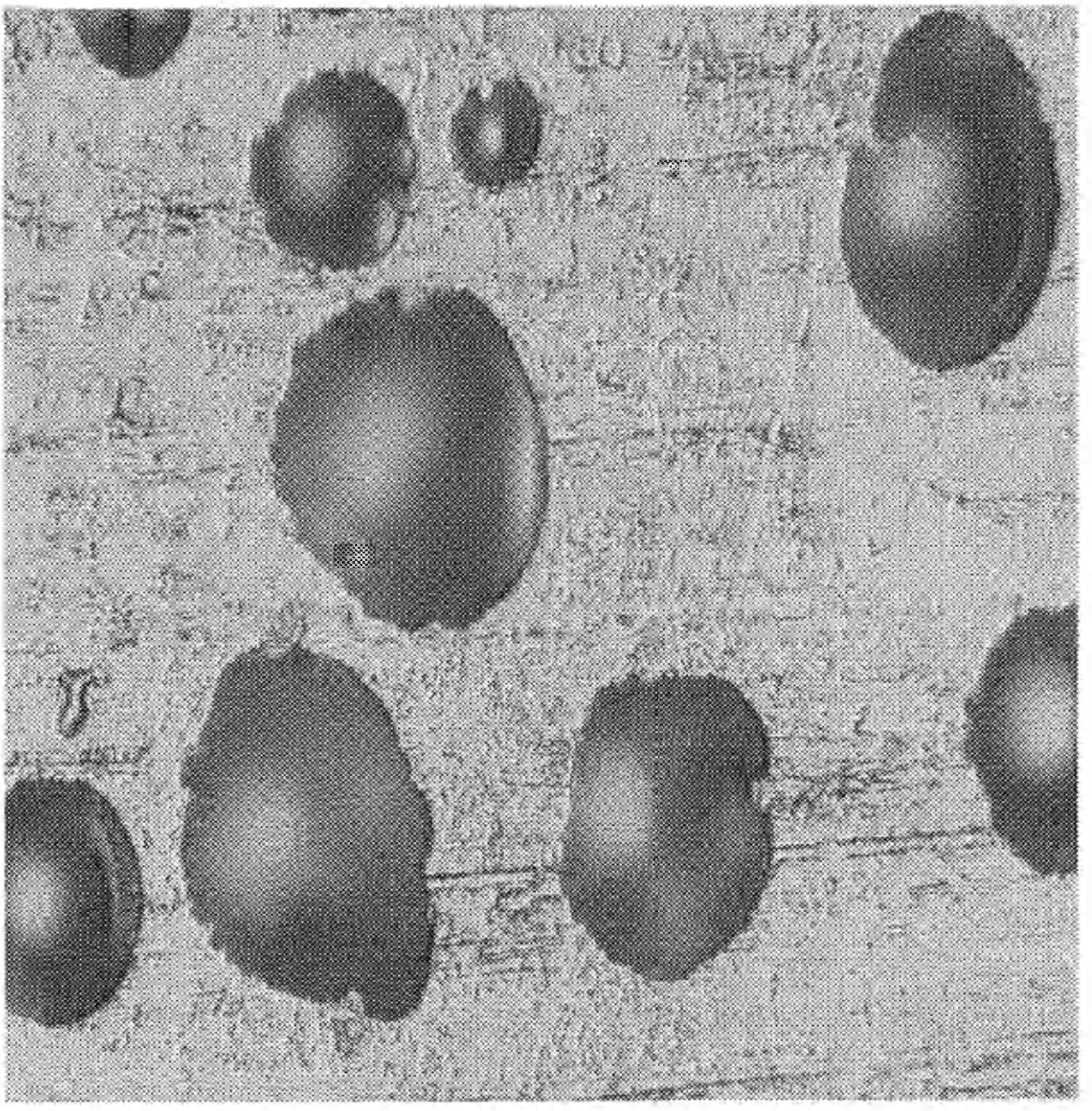

Figure 3.3 Photomicrograph of Dupont K3B with 20% B_4C Whiskers
Porosity is apparent in this photomicrograph of Dupont K3B as are B_4C whiskers. (200X)

Figure 3.4 Photomicrograph of PETI-5 (Pure)
(200X)

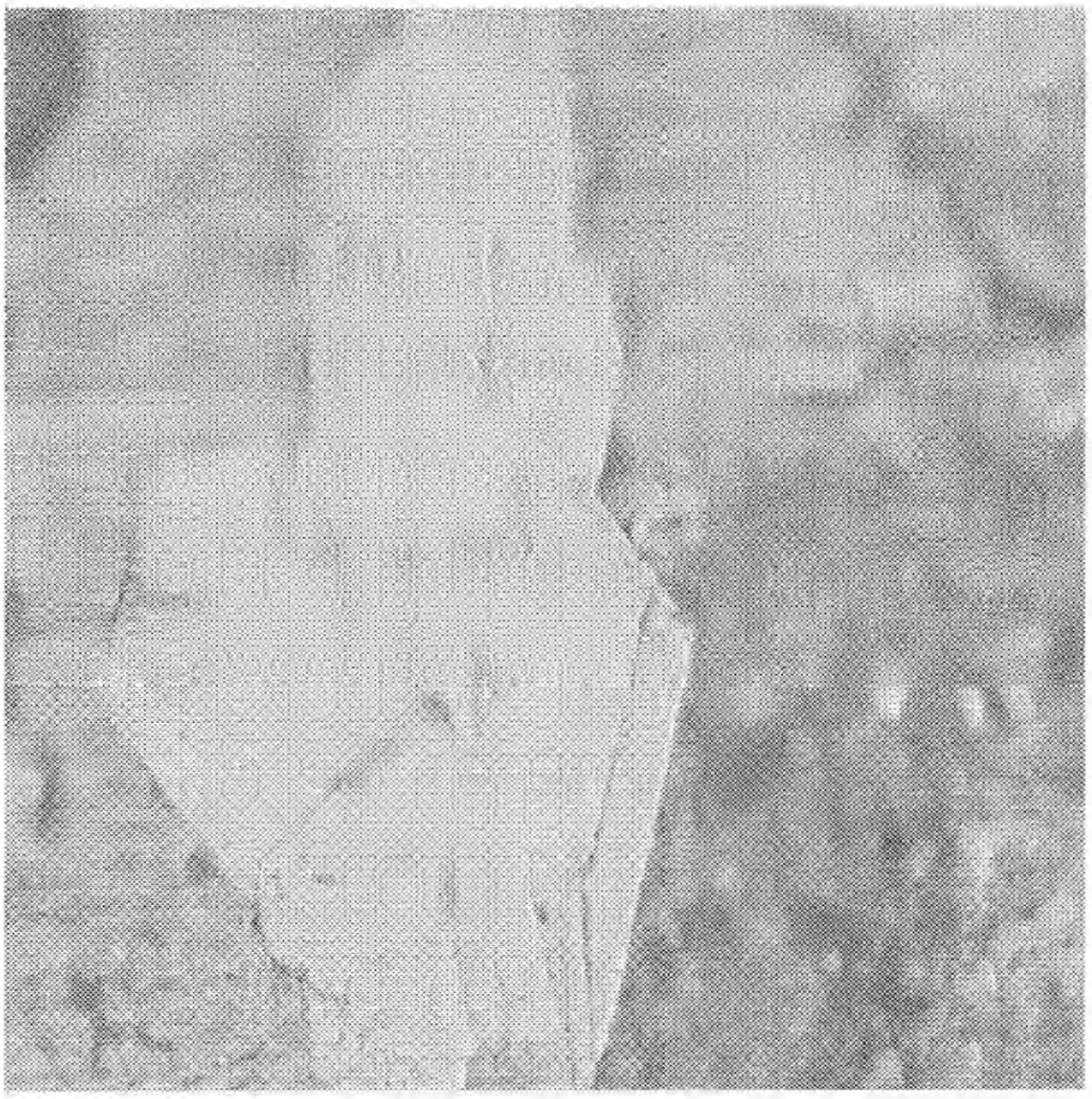

Figure 3.5 Photomicrograph of PETI-5 with 20% Amorphous Boron
A crystalline structure, believed to be a boron crystal, is apparent in this photomicrograph. (500X)

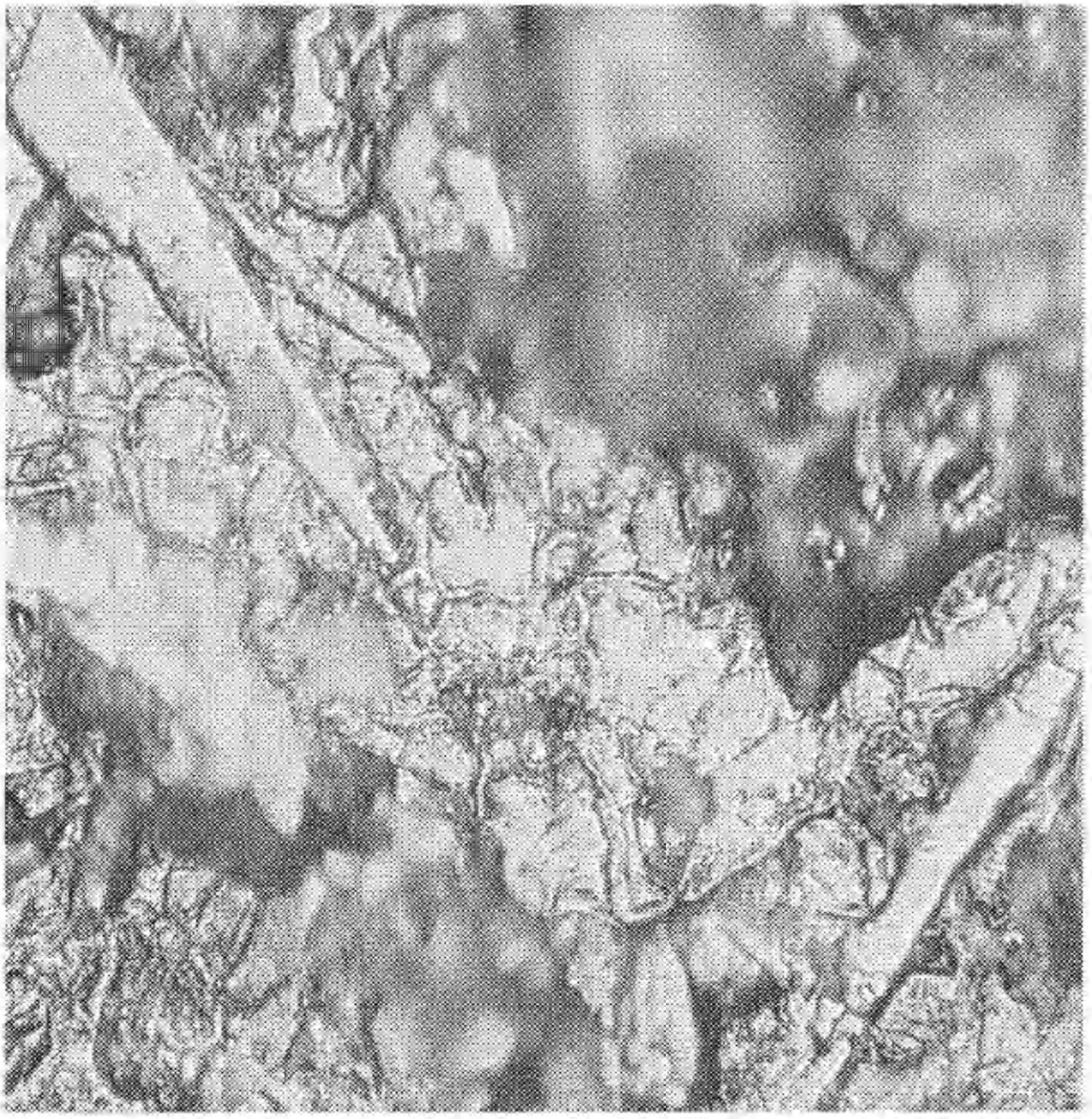

Figure 3.6 Photomicrograph of PETI-5 with 20% B_4C Whiskers
Boron Carbide whiskers are seen in this photomicrograph of PETI-5.
(200X)

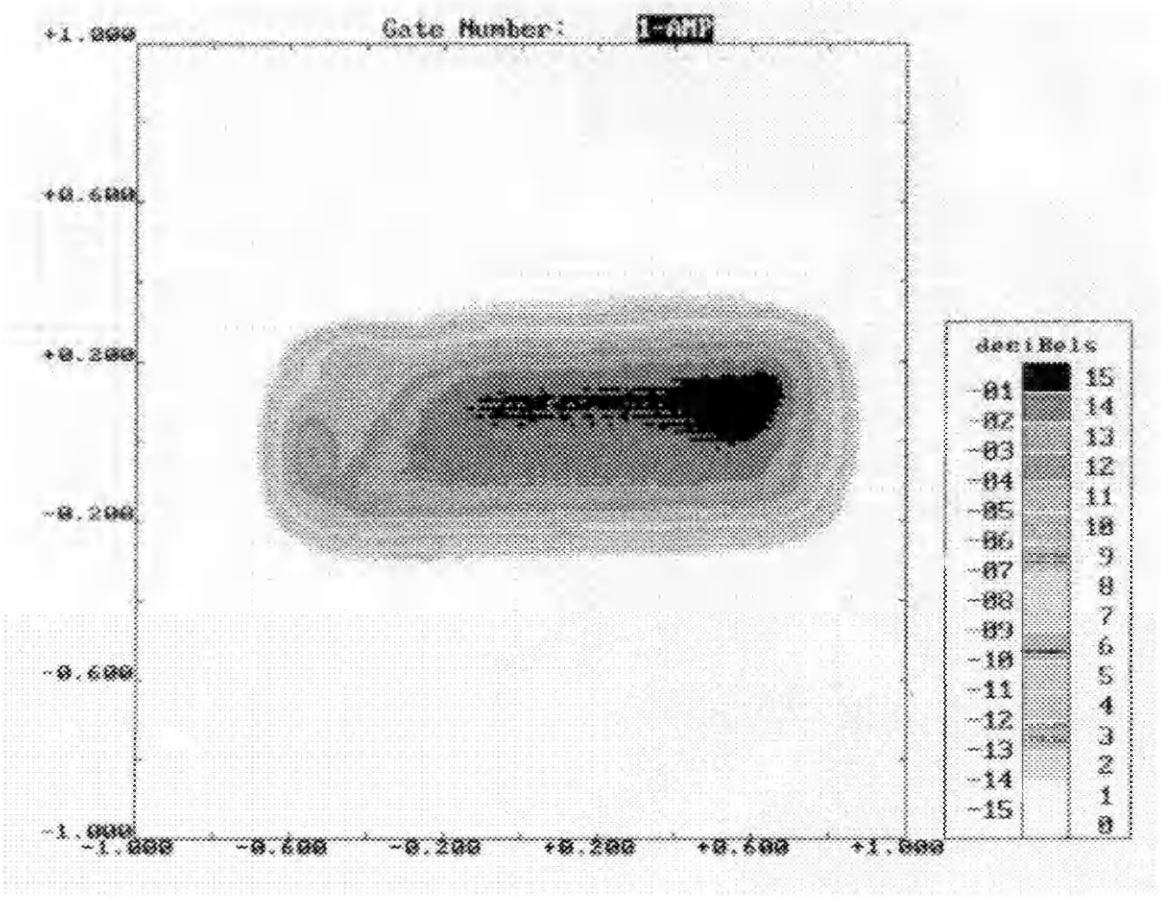

Figure 3.7
Ultrasound Scan
of PETI-5 Pure

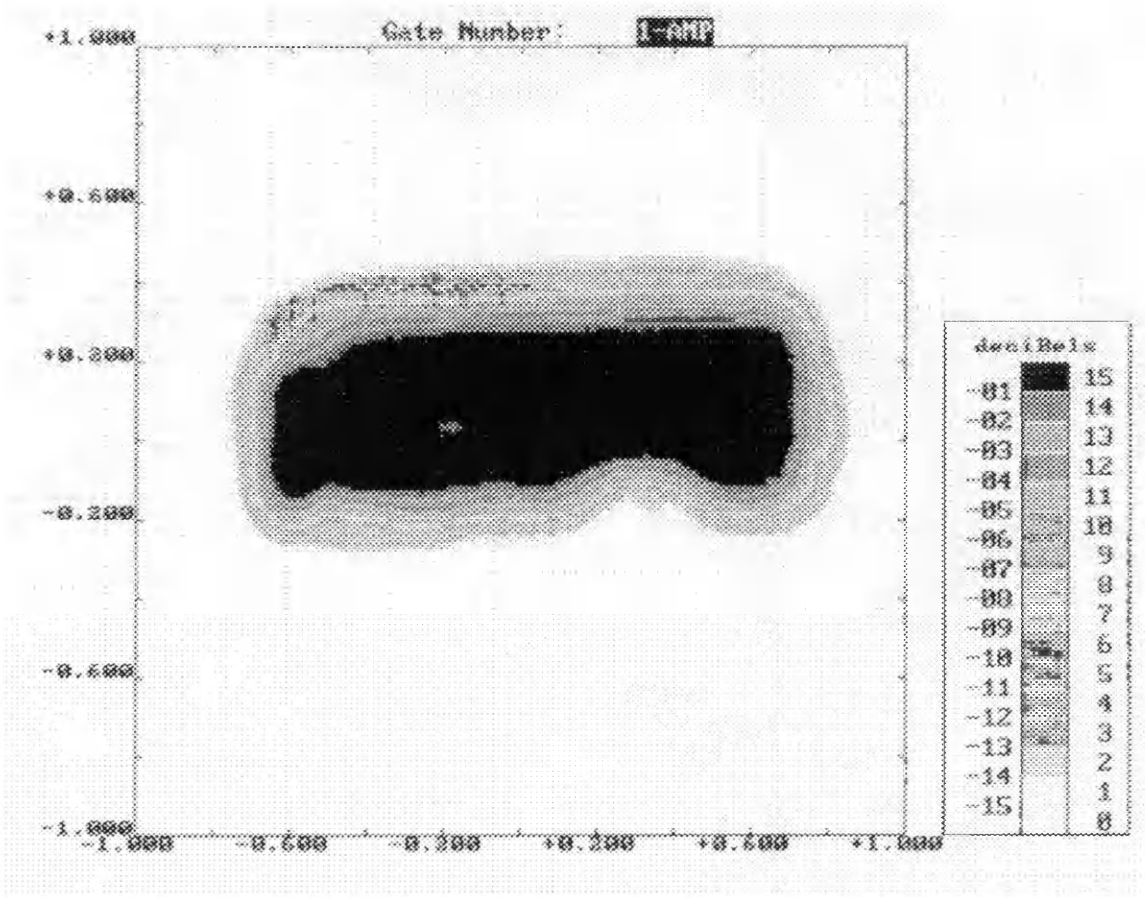

Figure 3.8
Ultrasound Scan
of PETI-5 with
20% Boron Carbide Whiskers

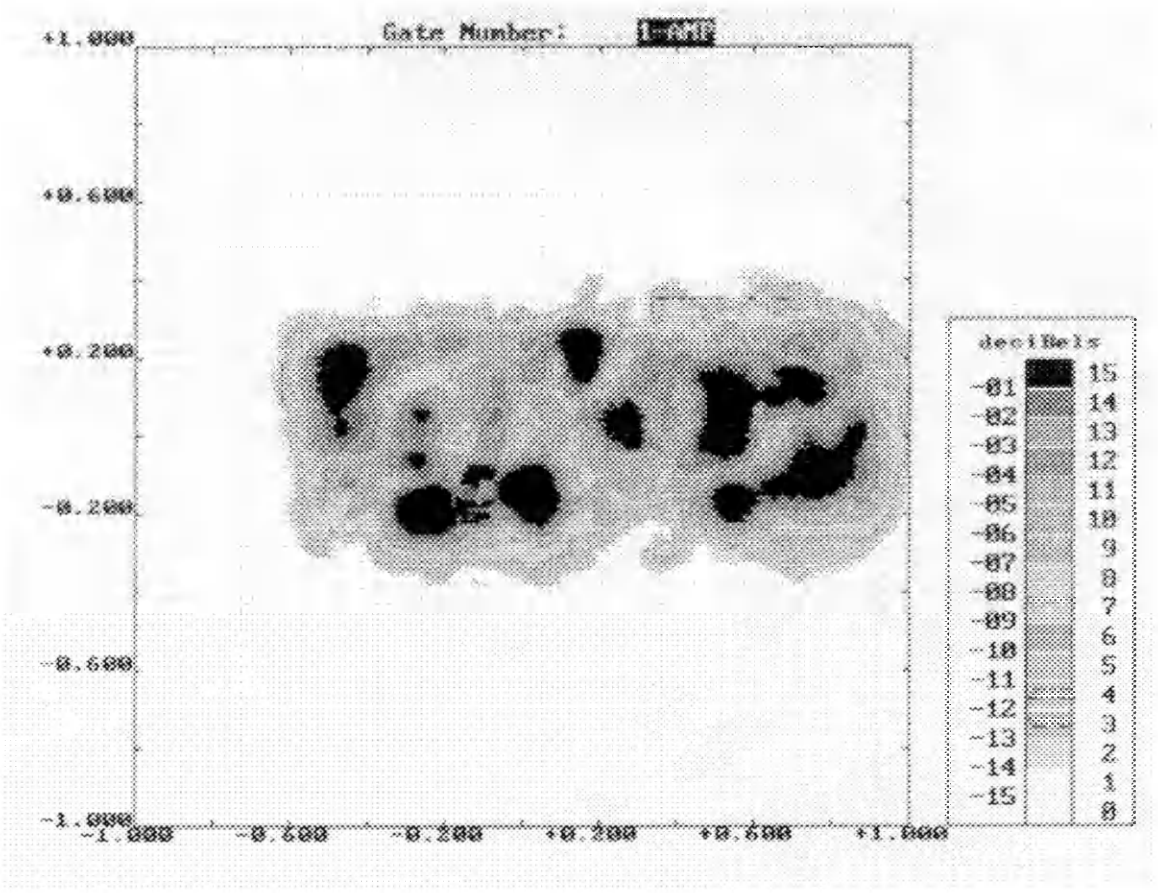

Figure 3.9
Ultrasound Scan
of K3B Pure

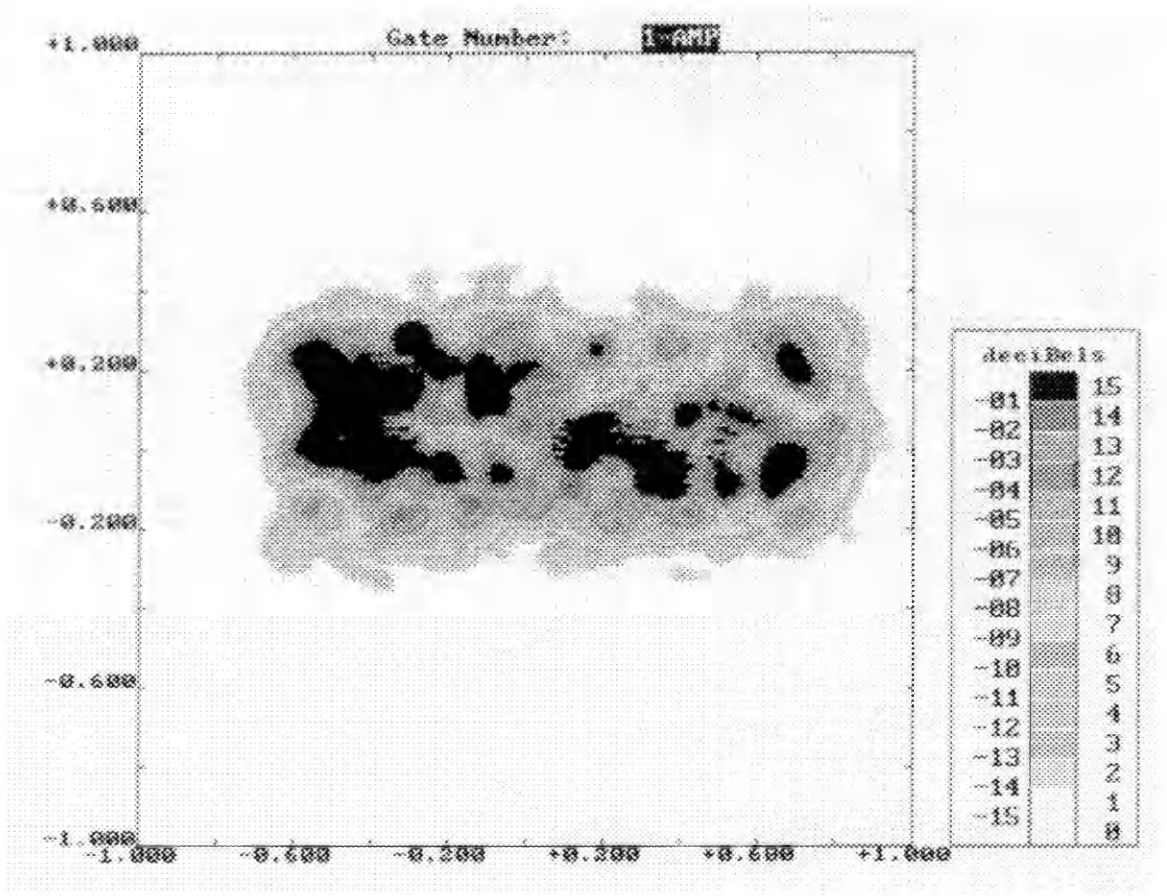

Figure 3.10
Ultrasound Scan
of K3B with
20% Amorphous Boron

DSC OF PURE PETI-5

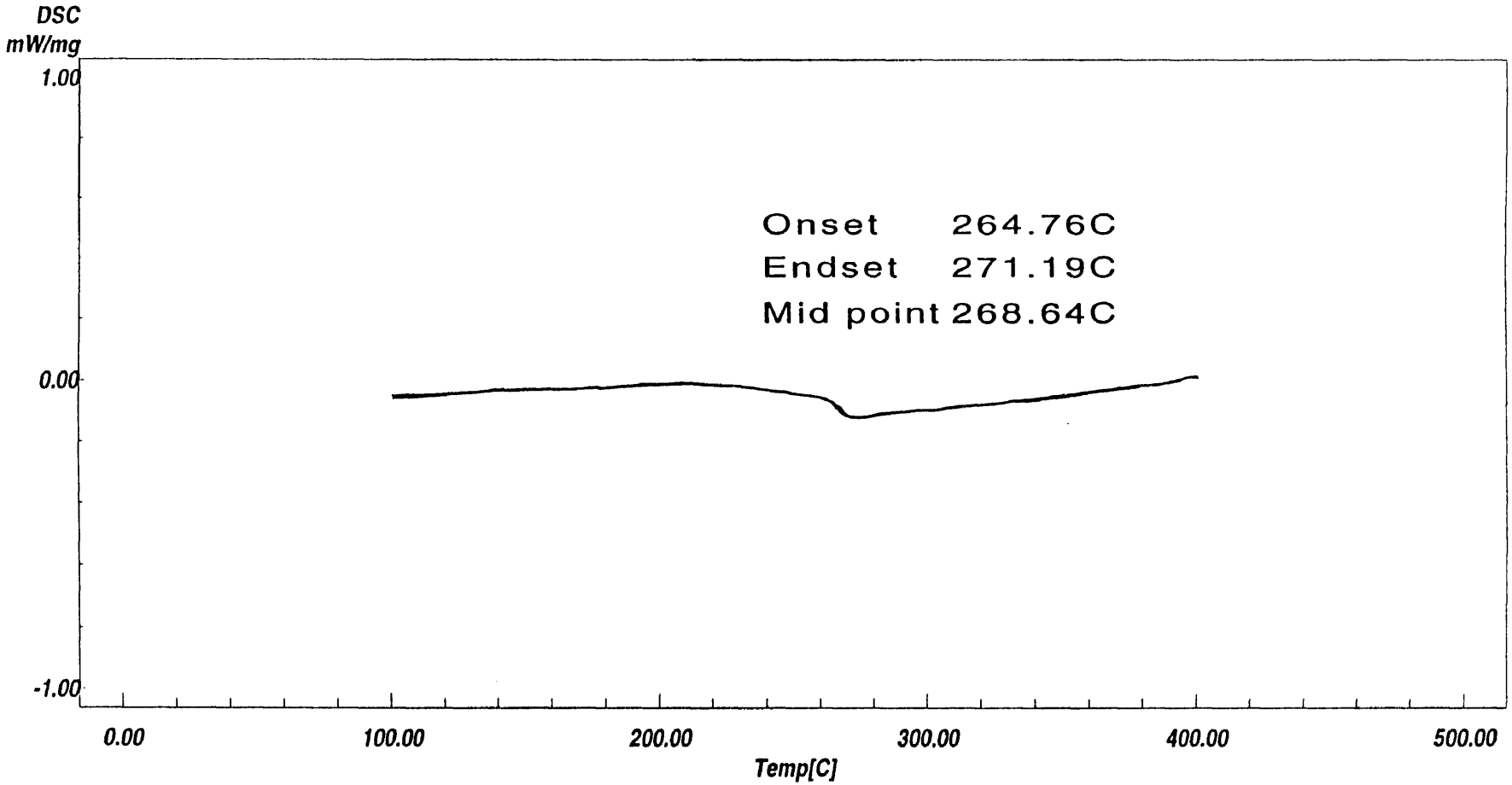

Figure 3.11

DSC Thermogram of PETI-5 Pure

DSC OF PURE K3B

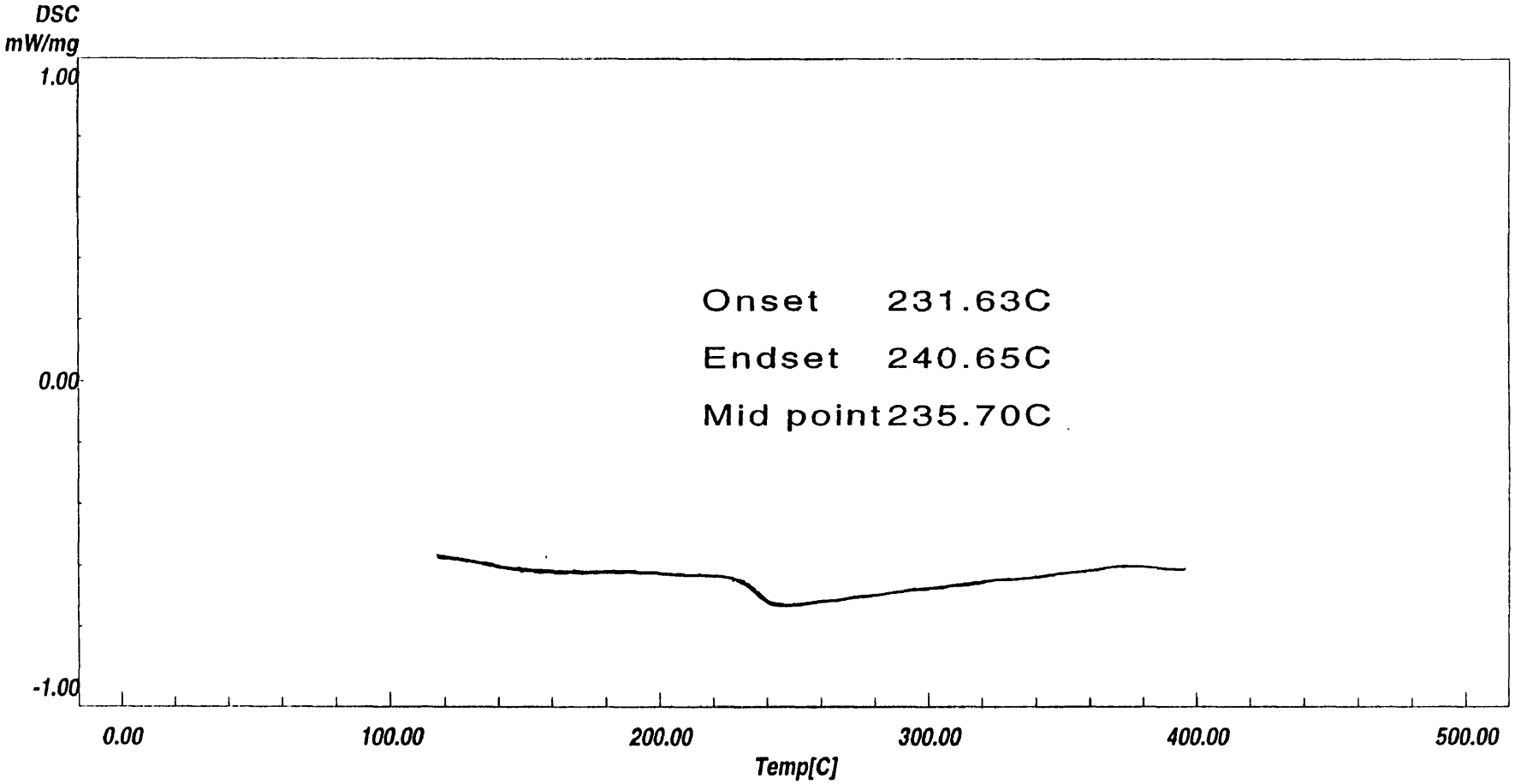

Figure 3.12

DSC Thermogram of K3B Pure

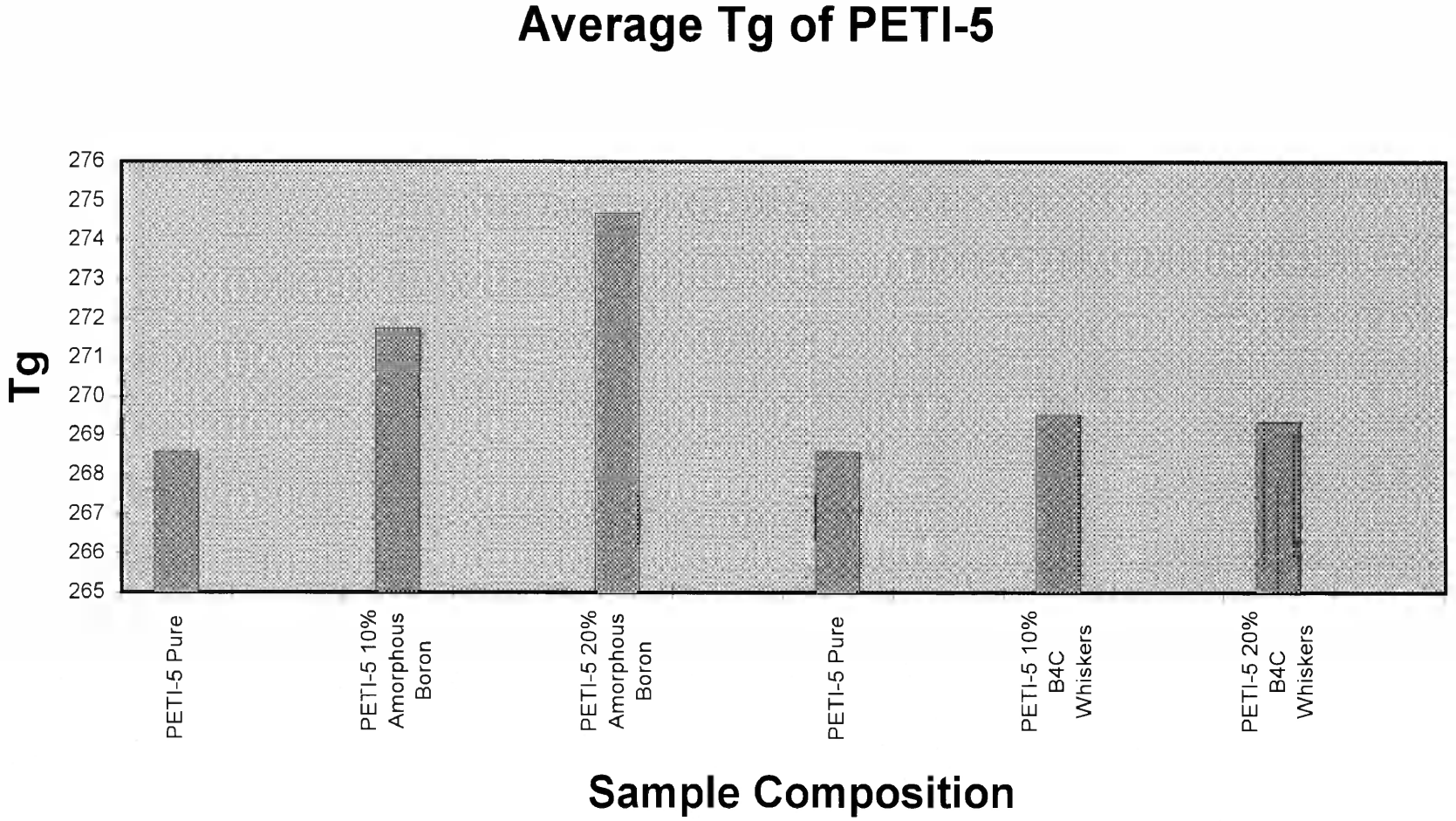

Figure 3.13
Tg of PETI-5 Materials

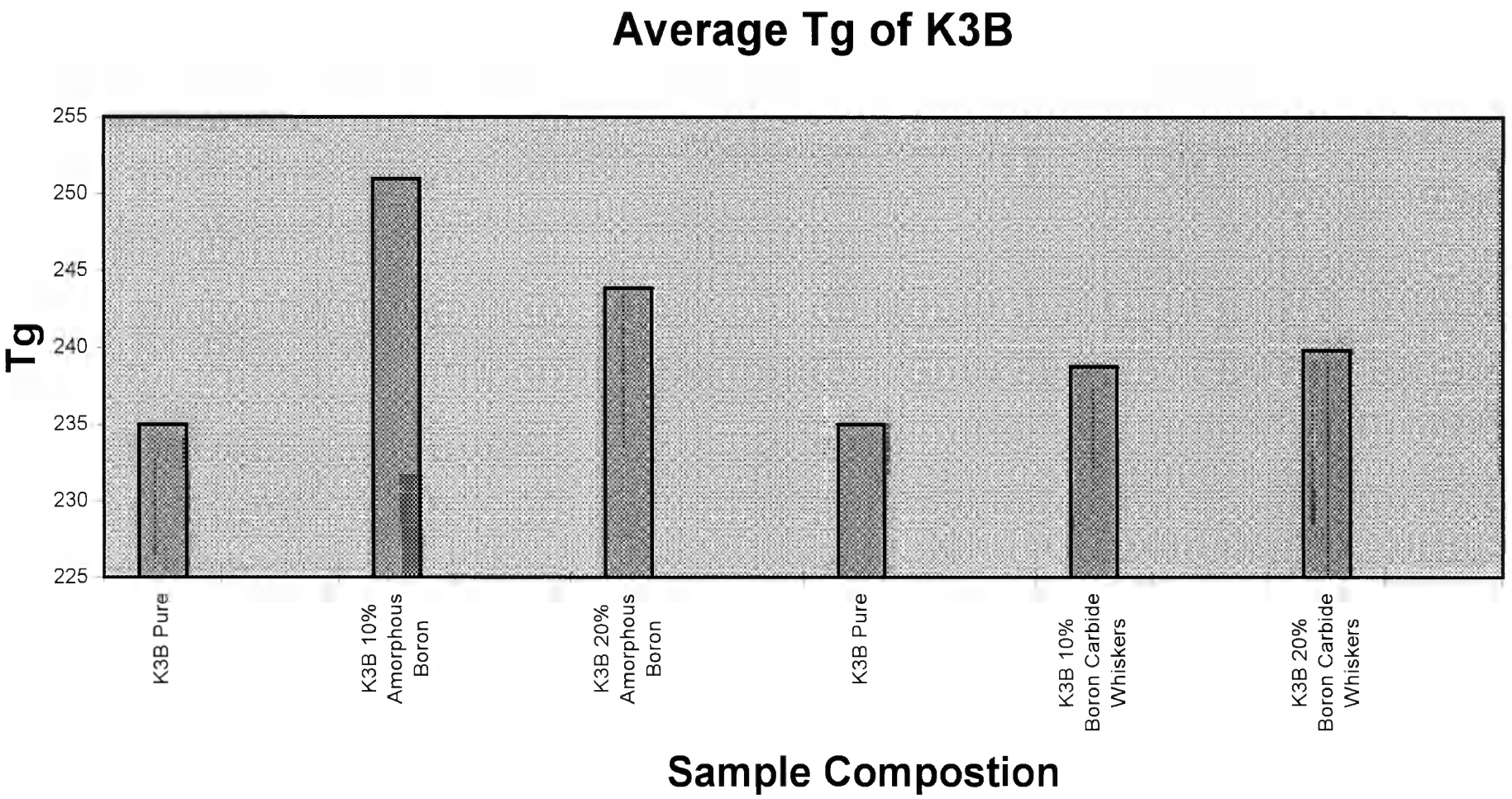

Figure 3.14
Tg of K3B
Materials

TGA of PETI-5 with 10% Boron Carbide Whiskers

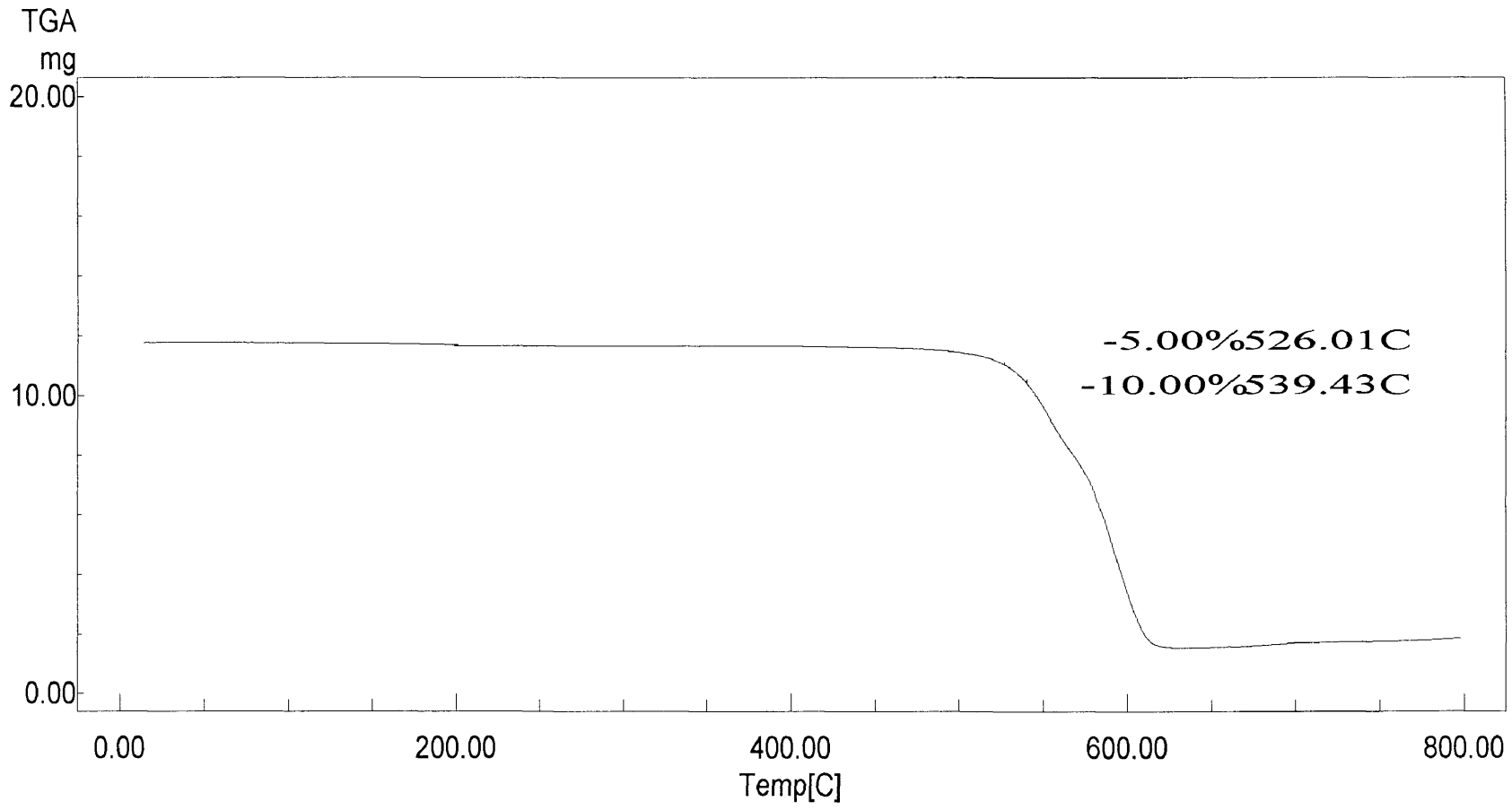

Figure 3.15

TGA Curve for PETI-5 with

10% Boron Carbide Whiskers

TGA of K3B with 10% Boron Carbide Whiskers

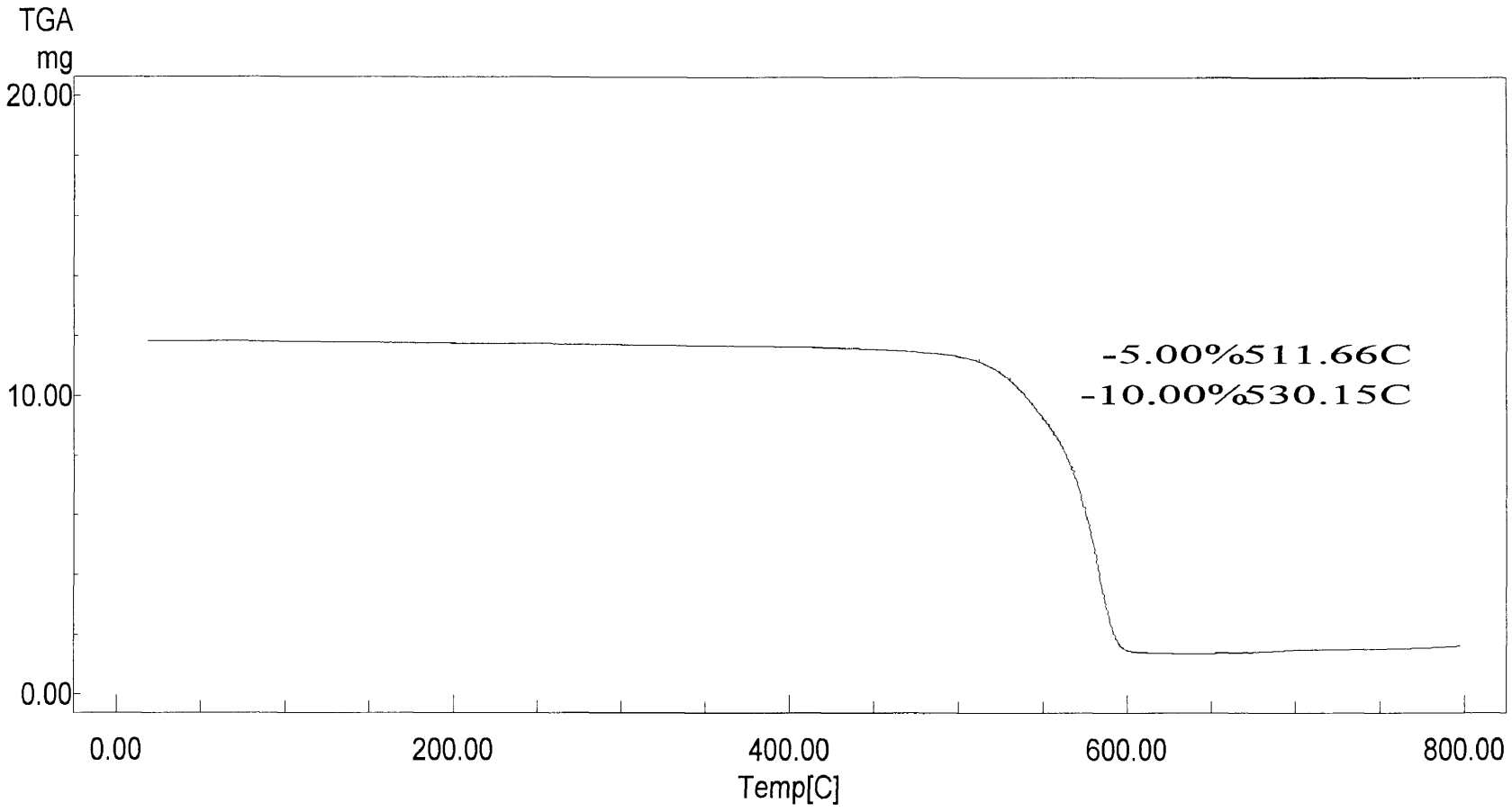

Figure 3.16

TGA Curve for K3B with

10% Boron Carbide Whiskers

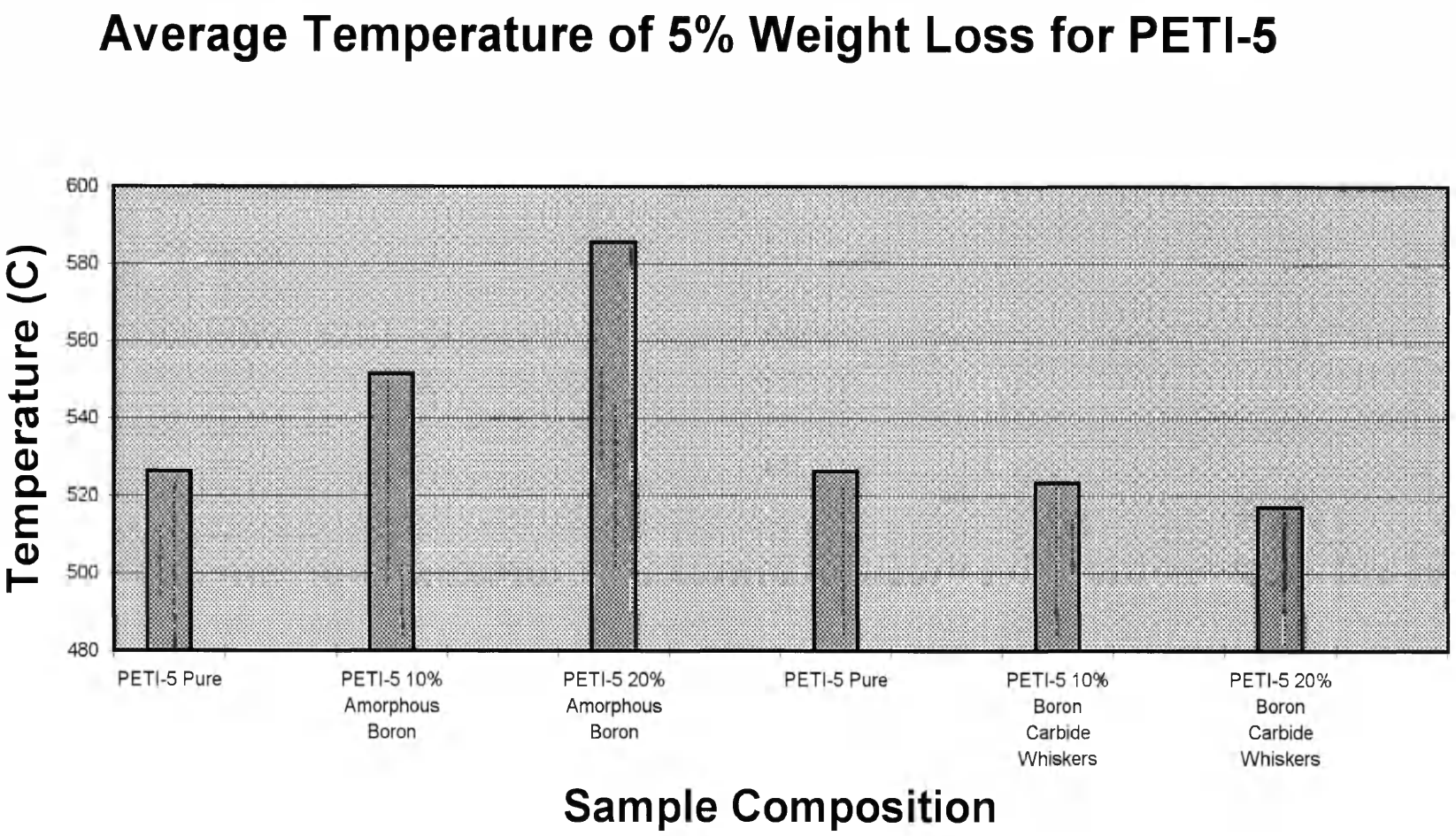

Figure 3.17
TGA of PETI-5 Materials

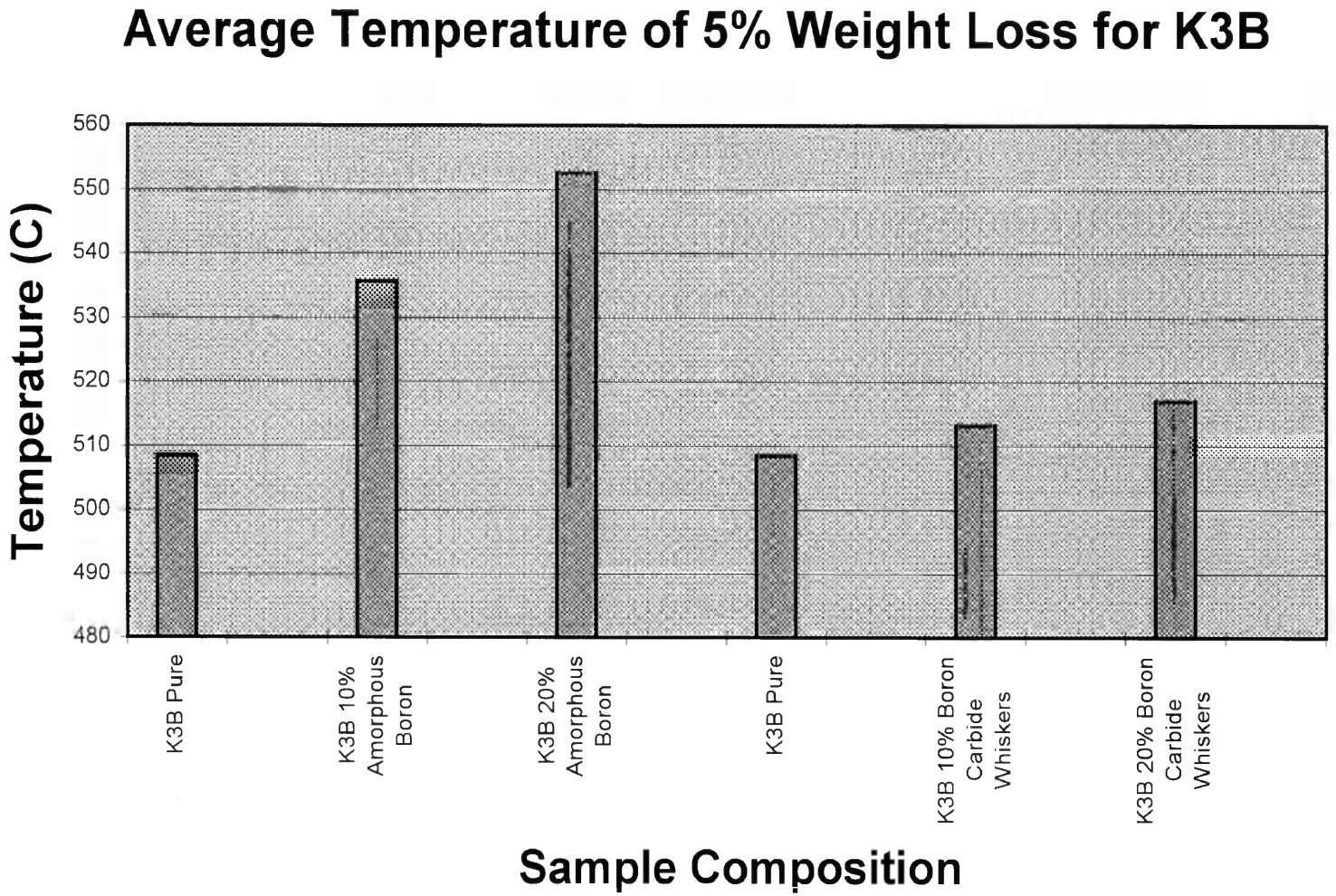

Figure 3.18
TGA of K3B
Materials

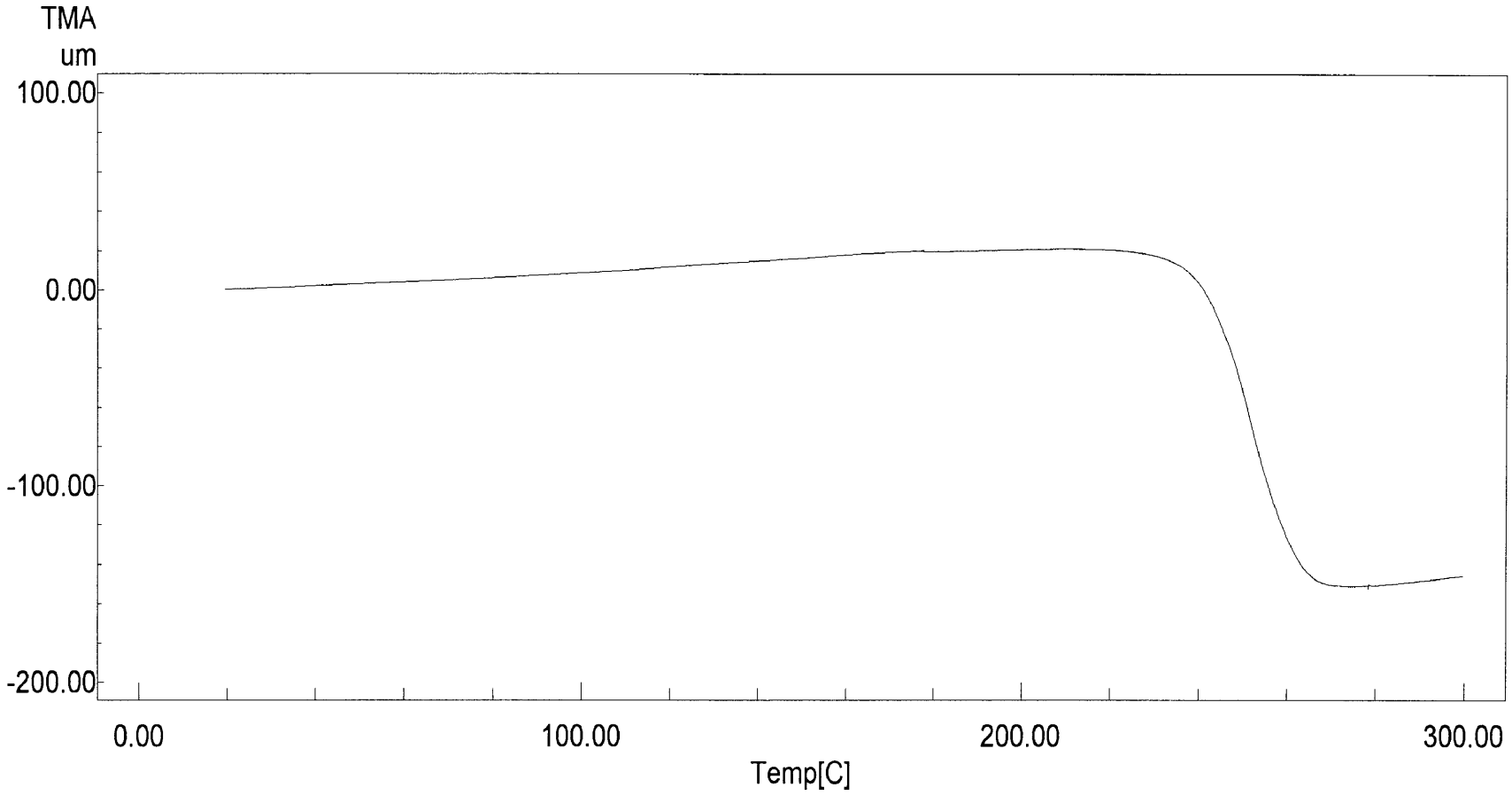

Figure 3.19

TMA Curve for PETI-5 with

20% Amorphous Boron

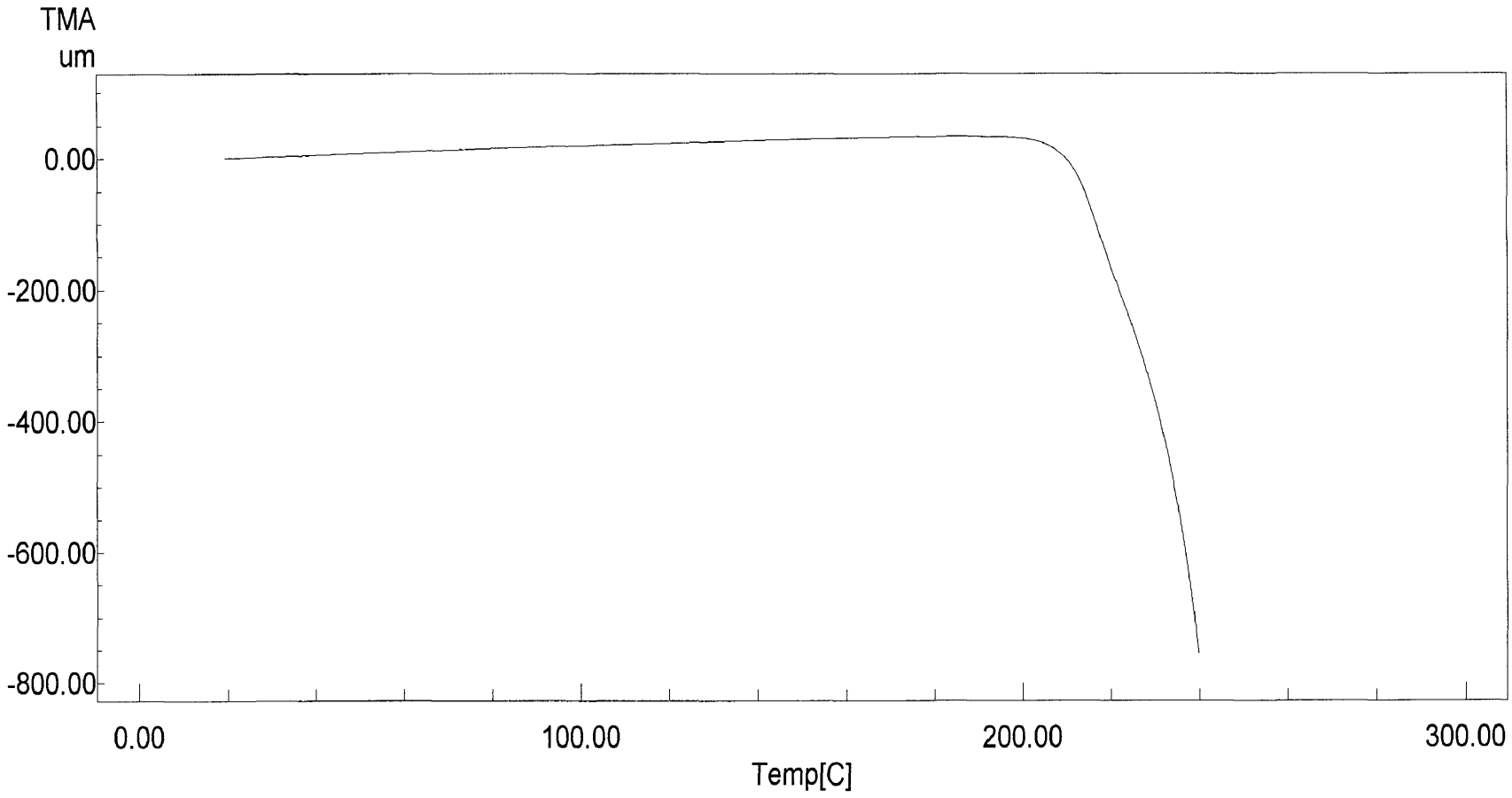

Figure 3.20

TMA Curve for K3B with

20% Amorphous Boron

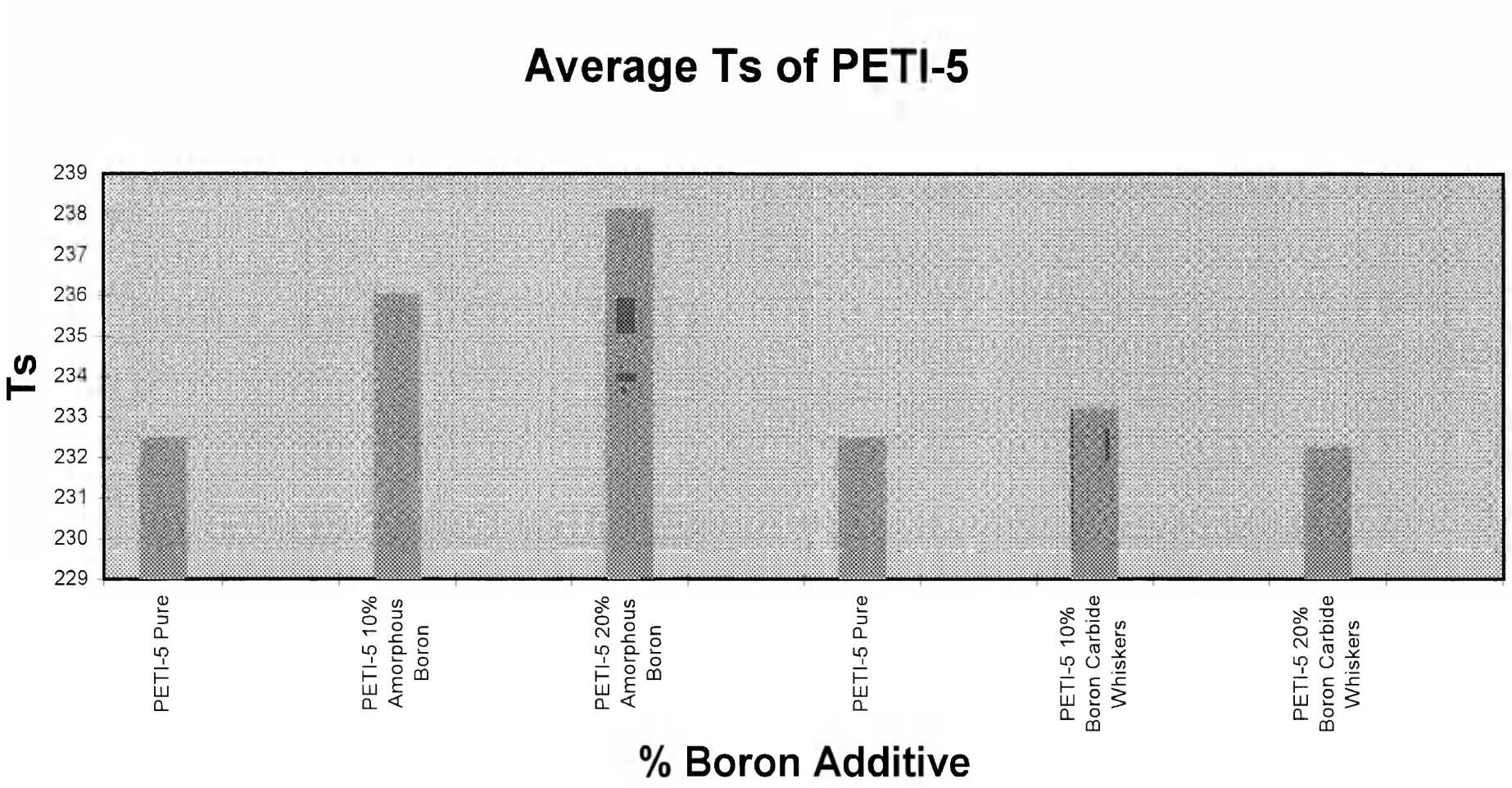

Figure 3.21
TMA of PETI-5 Materials

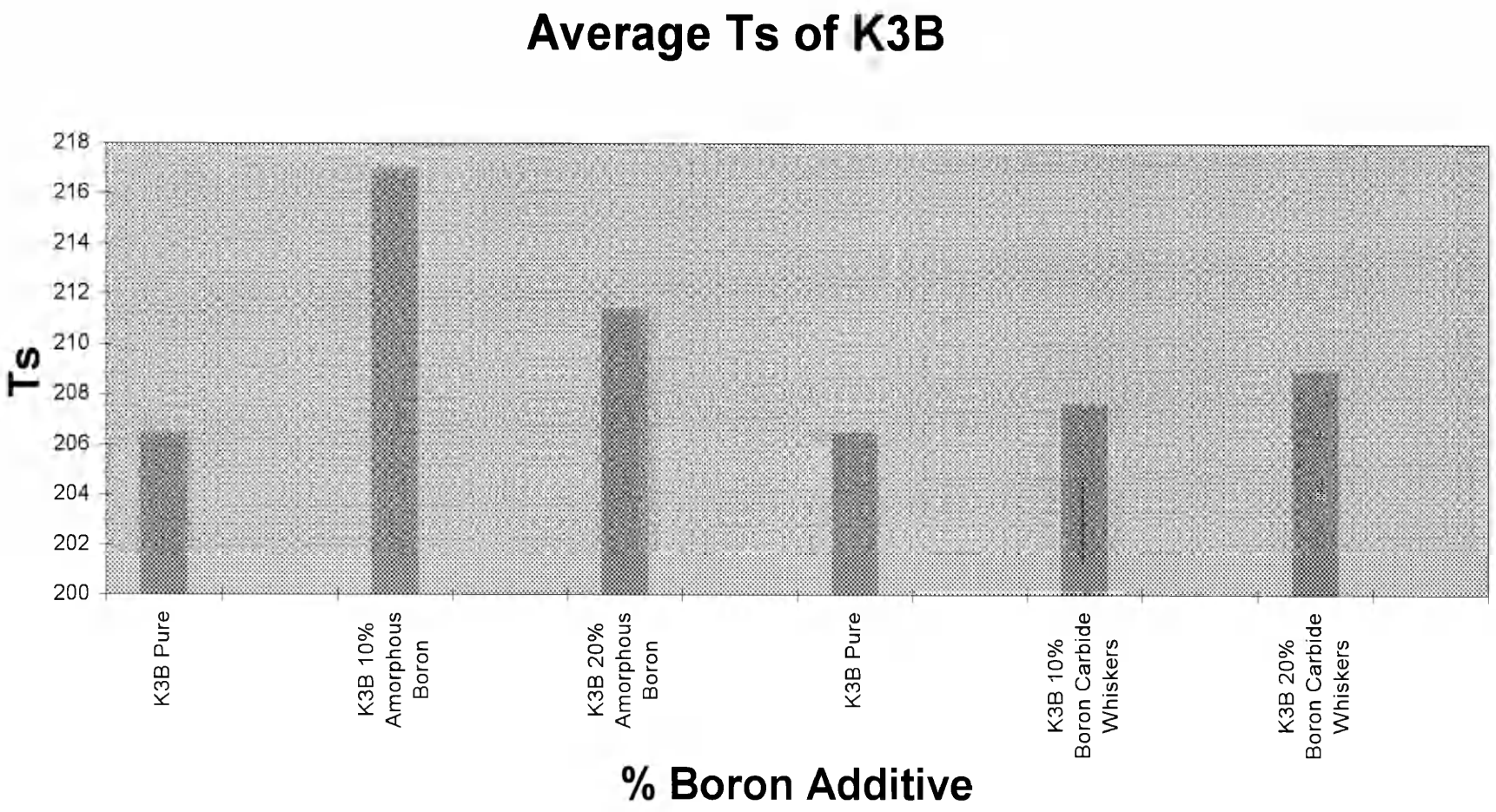

Figure 3.22
TMA of K3B
Materials

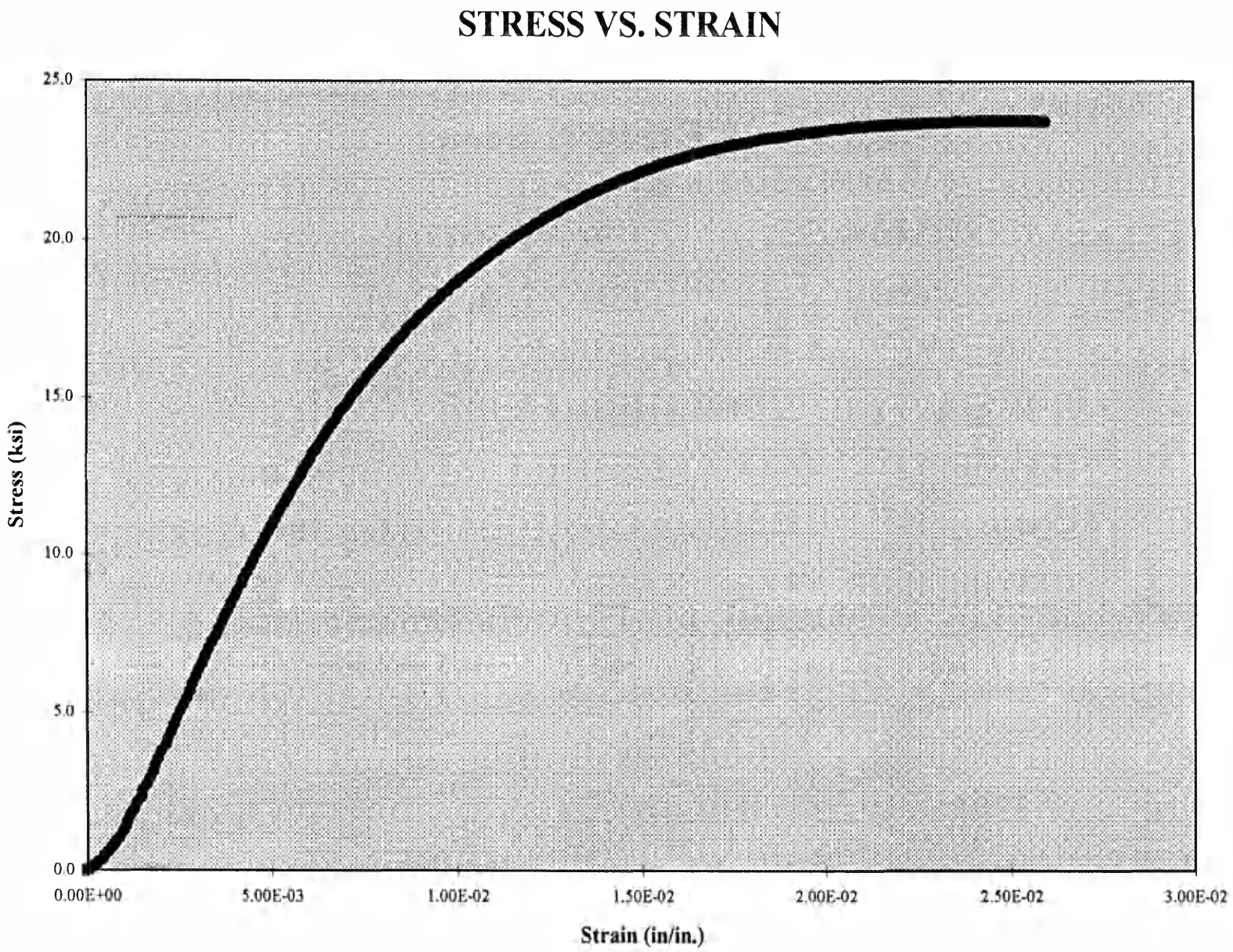

Figure 3.23
Stress vs. Strain Curve for PETI-5 (Pure)

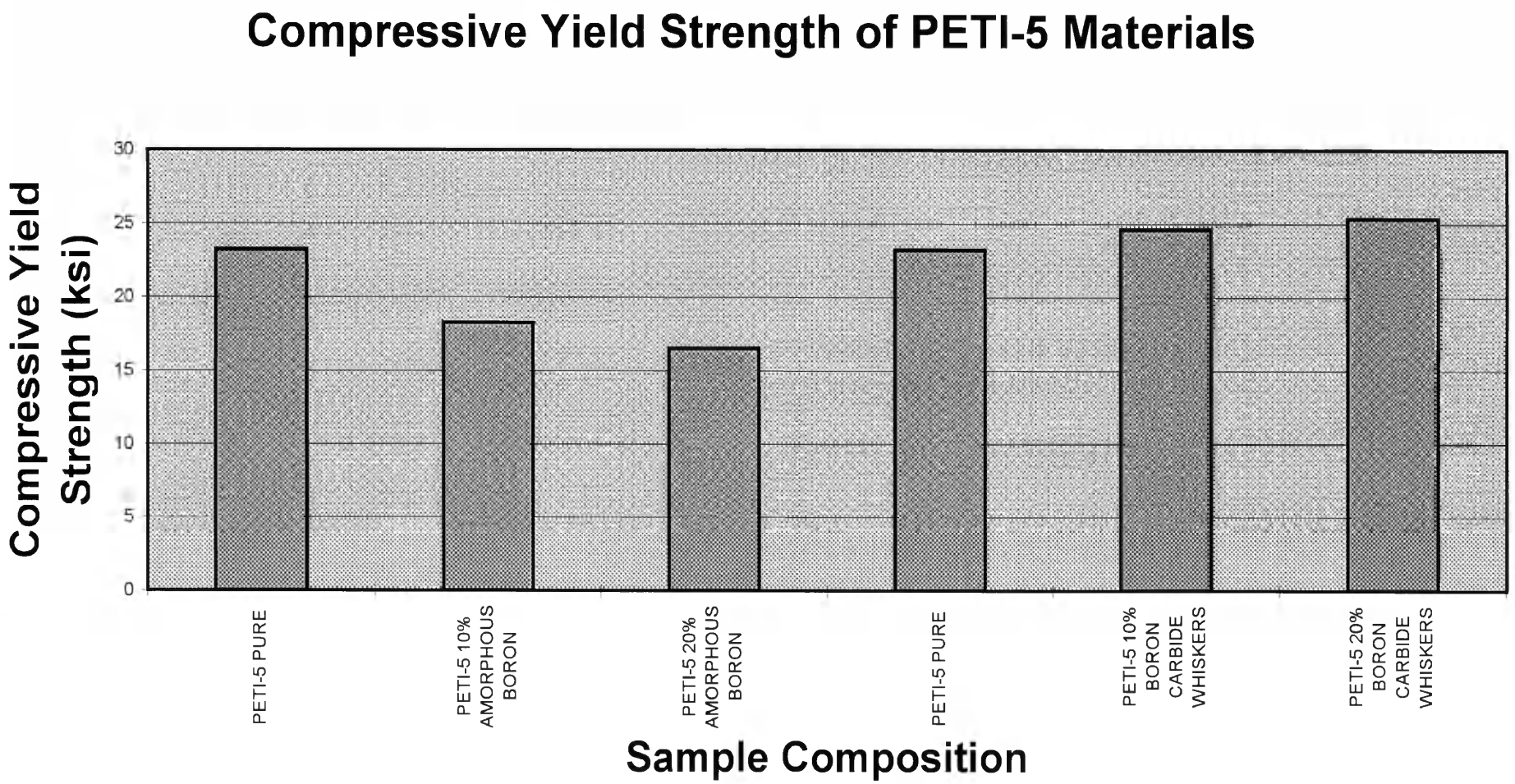

Figure 3.24
Compressive Yield Strength of PETI-5 Materials

Chapter IV.

Conclusions and Future Work

In this work, amorphous boron powder and boron carbide whiskers were added to two polyimides to enhance their radiation shielding capabilities. With an unusually high thermal neutron capture cross section, ^{10}B provides protection against the destructive effects of galactic cosmic radiation by offering shielding from neutrons.

Two different polyimides were chosen, NASA LaRC PETI-5 and Dupont K3B. PETI-5 is a phenylethynyl terminated thermoset, while K3B is a thermoplastic. Little was known about the chemical formulation of the Dupont K3B.

The PETI-5 was successfully processed with the addition of both amorphous boron and boron carbide whiskers. The addition of amorphous boron powder and boron carbide whiskers did not change the thermal properties significantly. In fact, amorphous boron powder enhanced the thermal stability of the polymer as well as the glass transition temperature.

The addition of amorphous boron powder and boron carbide whiskers did affect the mechanical properties of the

polymer. Amorphous boron powder lowered the compressive yield strength of the PETI-5. However, boron carbide whiskers enhanced the compressive yield strength as well as the compressive chord modulus of elasticity.

The Dupont K3B material was not successfully processed with the addition of amorphous boron powder and boron carbide whiskers. The molded samples contained voids and surface imperfections. The amorphous boron samples were especially brittle. Different approaches were taken to solve these problems, but these difficulties could not be overcome. They affected the mechanical data obtained. However, they did not affect the thermal data generated.

The mechanical data for the K3B polymer did not provide any useful information. The results differed by as much as 100% for two samples with the same concentration of boron additive. Therefore, the data were not included. The thermal analysis did provide useful information. As with the PETI-5, the addition of amorphous boron and boron carbide whiskers did not change the thermal properties of the polymer significantly.

In the future, mechanical testing will be continued on both polyimides. Flexure tests and tensile tests will be conducted to determine the effects of amorphous boron and boron carbide

whiskers on these mechanical properties. The boron carbide whiskers show great promise, as they are the ultimate in structural reinforcement. Neutron absorption studies will also be made to determine the level of radiation shielding provided by the boron additives.

In conclusion, PETI-5 with the addition of boron carbide whiskers seems to be very promising for space applications. The boron carbide whiskers are easily incorporated into the polymer matrix. The addition of the boron carbide whiskers does not change the excellent thermal properties of the polyimide. The high hydrogen content coupled with boron provides radiation shielding. Finally, the addition of boron carbide whiskers improves the compressive properties and hopefully other mechanical properties of the polyimide as well.

VITA

STEPHEN C. KO

The author was born in Norcross, Georgia, on October 16, 1973. He was graduated from Norcross High School in June of 1992 and from The College of William and Mary in May of 1996 with a Bachelor of Arts in Religion.

After earning his Master of Arts degree in Chemistry, he will enter medical school at the Silesian University Medical School in Katowice, Poland. There he will study medicine and prepare for his future as a pediatrician.